ITEA 2
INFORMATION TECHNOLOGY FOR EUROPEAN ADVANCEMENT

BENEFIT

Better Effectiveness and Efficiency by Measuring and Modelling Interventional Therapies

DELIVERABLE D7.3
State of the art on selected clinical procedures and intra-interventional imaging techniques

Project number:	ITEA 13031
Document version no.:	v 1.0
Edited by:	Herman Stegehuis (Philips Healthcare)

ITEA Roadmap domains:
Major: Group

ITEA Roadmap categories:
Major: Content & knowledge
Minor: Interaction

HISTORY

Document version #	Date	Remarks
V0.1	July 24, 2017	Starting version, template
V0.2	July 28, 2017	Medis, added text to section 4.2.4.
V0.3	Sept 13, 2017	Input Barco, Demcon, Philips added
V0.4	Oct 10, 2017	Various inputs added
V0.5	Oct 17, 2017	Input Elekta, Quantib, Linköping University
V0.6	Oct 25, 2017	FEops: 4.1.4
V0.7	Nov 9, 2017	LUMC: 4.1.4
V1.0	Nov 9, 2017	Approved

Deliverable review procedure:

- **4 weeks before due date**: deliverable owner sends deliverable –approved by WP leader– to Project Manager.
- **Upfront** PM assigns a co-reviewer from the PMT group to cross check the deliverable
- **2 weeks before due date**: co-reviewer provides input to deliverable owner
- **Due date:** deliverable owner sends the final version of the deliverable to PM and co-reviewer

TABLE OF CONTENTS

1 Executive summary

This document provides the “State of the Art” for the clinical procedures and the imaging technologies which have been targeted by the BENEFIT project. The goal of BENEFIT was to develop technologies that improve efficiency and effectiveness of minimally invasive interventional procedures based on improved quantification and modeling before, during and after interventions, whereby imaging is used as one of the major tools.

This deliverable D7.3 is a compilation of the earlier public SotA documents
- D1.1.1 State of the art on models for patient risk stratification,
- D4.1.1 State of the art on Intra-interventional Imaging, and
- D4.3.2 State of the art on real-time devices and navigation

and adds the progress as made during the BENEFIT project.

In total 5 clinical procedures are addressed:
- Heart valve procedures
- Treatment of (partially) blocked arteries causing ischaemia or infarct of the heart
- Treatment of blocked or ruptured brain arteries
- Treatment of liver tumors
- Treatment of brain tumors

Additionally 4 imaging techniques are addressed:
- High Quality X-ray Imaging
- Intravascular Ultrasound and Optical Coherence Tomography
- MRI and Cone-beam CT
- Laparoscopic Imaging

As such, the spectrum of selected topics cover a broad range of minimally invasive interventional procedures.

2 Introduction

2.1 Aim of activity

The goal of this document is to provide a state-of-the-art review on selected clincial applications and medical imaging techniques which have been a topic of investigation in the ITEA2 BENEFIT project. It brings together the earlier State of the Art deliverables D1.1.1 and D4.1.1 and adds to it an update with the BENEFIT results in one single overview document.

Both previous SotA deliverables were based on open literature, the knowledge provided by the clinical partners of the project and additional clinical consultants. The updates due to BENEFIT have been partly published in scientific articles, conference proceedings or commercial brochures.

Chapter 5 describes each of the targeted interventions in a standardized way. The first section provides the background of the disease and the procedure, the second section describes the existing way of working, the third section reviews the state of the art on risk stratification, intervention selection and procedural success evaluation. The new fourth section describes progress due the BENEFIT project with an emphasis on the clinical aspects.

Similarly chapter 7 describes state of the art in intra-interventional imaging as in D4.1.1: introduction, technical state of the art, usage in intervention and treatment evaluation. The 4th section is again on the progress during BENEFIT but in this case with an emphasis on the technical aspects.

2.2 Contributors

Several authors from the BENEFIT partners contributed to the production of this document. We are indebted for the contributions from our Clinical consultants.

#	**Section**	**Author**	***Clinical consultant***	***Medical Center***
1	Valvular Assessment and treatment	LUMC, FEops	Philippe Bertrand	ZOL, Belgium
2	Percutaneous Coronary Interventions	LUMC, Medis, Philips	Wouter Jukema R. Bullens, Clinical Scientist	LUMC Philips
3	Brain vessel interventions	EMC, Philips	Dr. B.J. Emmer, neuroradiologist T. Grunhagen, Clinical Scientist	Erasmus MC Philips
4	Liver tumor treatment	DEMCON, EMC, Philips, UMCU	S. Klink, Interventional Radiologist M.S. van Leeuwen, Radiologist A. Radaelli, Clinical Scientist	Erasmus MC UMC Utrecht Philips
5	Brain tumors	Elekta, Quantib, Linkoping Univ,	Joel Goldwein, MD & Sr VP Clinical Affairs M. Smits, MD, neuroradiologist	Elekta Erasmuc MC

3 Glossary

3DRA	3 Dimensional Rotational Angiography: 3D X-ray imaging of blood vessels
ADC	Apparent Diffusion Coefficient
AR	Aortic regurgitation: back flow of blood from aorta into heart (leakage of aortic valve)
AS	Aortic stenosis: narrowing in aorta
CABG	Coronary Artery Bypass Graft(ing): surgery to place a bypass vessel across an obstructed blood vessel of the heart
CBCT	Cone Beam CT: CT reconstruction made by an interventional X-ray system instead of a dedicated CT scanner
CT	Computer Tomography: method to mathematically reconstruct 3D images from a rotational sequence of 2D X-ray slices
CFR	Coronary Flow Reserve: measure for condition of vessels of the heart
CTA	Computer Tomography Angiography: 3D imaging of blood vessels with CT after injection of a contrast agent into a vessel.
CTO	Chronic Total Occlusion
DSA	Digital Subtraction Angiogram: 2D X-ray imaging of blood vessels after injection of a contrast agent
DWI	Diffusion Weighted Imaging: specific protocol of MRI
FFR	Fractional Flow Reserve: measure for condition of vessels of the heart
Fr	French, a catheter scale: 1 Fr = 0.33 mm
GUI	Graphical User Interface
HMI	Human Machine Interfaces
IGIT	Image Guided Interventional Therapy
IVUS	IntraVascular UltraSound: imaging of a vessel wall from the inside with a US transducer mounted on the tip of a catheter
LGE-MRI	Late Gadolinium Enhancement MRI
LV	Left ventricle
Mediate	patient friendly MEDIcAl inTErvention: predecessor ITEA project
MR	Mitral regurgitation: back flow of blood from left ventricle aorta into atrium due to leakage of mitral valve
MRI	Magnetic Resonance Imaging
MR-HIFU	MRI-guided High Intensity Focused Ultrasound
MS	Mitral stenosis: narrowing of miral valve due to calcification
MW	MicroWave
OCT	Optical Coherence Tomography: imaging modality using laser pulses for high resolution imaging of a surface, for instance the vessel wall
OR	Operating Room
PCI	Percutaneous Coronary Intervention: minimally invasive treatment of obstruction in cardiac blood vessel via a catheter
PEI	Percutaneous Ethanol Injection
QCA	Quantitative Coronary Angiography
RF(A)	Radio Frequency (Ablation): removal of tissue by heat
SPECT	Single Photon Emission Computed Tomography: 3D imaging of molecular processes in the body after injection of a radio-isotope
SSS	Symptom Severity Score
TAVI	Transcatheter Aortic Valve Implantation: implantation of artifical heart valve via a catheter (so no open surgery)
TEE	Transesophageal echocardiography: US imaging of the heart with a

	transducer mounted on a tube that is inserted in the esophagus
TTE	Transthoracic echocardiography: US imaging of the heart with a transducer on the chest in between of 2 ribs
US	UltraSound
VHD	Valvular heart disease

4 Clinical Procedures

The clinical use cases on PCI and heart valve treatment in BENEFIT have also been described in the ITEA-2 Mediate project that ended in December 2013. Parts of the clinical introduction for these use cases have been taken from the State of the Art document of Mediate (Aerts, 2011).

4.1 Valvular Assessment and Treatment

Lead authors: FEops & LUMC

4.1.1 Introduction

Valvular heart disease (VHD) is a common public health burden in the developing and industrialized countries. The increasing life expectancy in the western world has resulted in an increasing prevalence of VHD. Diagnosis and treatment of patients with valvular disease is complex as symptoms of the disease may often reveal at a late stage while early treatment is key to optimal prognosis for the patient. Each of the four heart valves may be affected. A valve may be narrowed/hardened (referred to as valvular stenosis) due to fibrosis and calcification, or may be leaking (referred to as valvular regurgitation or insufficiency). In both situations the valve disease may influence cardiac function and remodeling. A stenosed aortic valve may result in a depressed left ventricular ejection fraction and the development of left ventricular hypertrophy due to the higher afterload for the left ventricle. Mitral valve insufficiency on the other hand may result in left ventricular and/or left atrial dilatation leading to heart failure, increased risk of cardiac arrhythmias, increased pulmonary resistance and increased end-systolic right ventricular pressure.

In Europe aortic valve stenosis (33.9%) is the most common form of VHD, followed by mitral regurgitation (24.8%), aortic regurgitation (10.4%) and mitral stenosis (9.5%). Right sided VHD is much less common (1.2%) (Iung, 2003). The following sections provide a brief summary on the clinical state of the art related to left sided VHD followed by a description on the state of the art related to the currently available methods and guidelines for risk stratification, treatment planning and success evaluation for clinical management of left sided VHD.

4.1.2 Clinical State of the Art

Diagnosis and detailed assessment of the severity of valvular disease includes various examinations. Routine clinical examination may reveal distinctive heart sounds (murmurs) which are used as indicators of VHD. It has been shown however that clinical examination alone is not a reliable guide to diagnosis or severity grading. The gap in the clinical diagnosis of VHD and the late presentation of many patients with severe disease emphasizes the importance of quantitative, high-quality cardiac imaging. Depending on the specific situation a patient may need to undergo several additional tests in order to obtain an accurate assessment of the severity of the valvular pathology. Currently, cardiac ultrasound (US) is the clinical workhorse for anatomical and functional assessment of the cardiac valves. Transthoracic echocardiography (TTE) is routinely performed during a cardiac examination and is the cornerstone for the diagnosis of valvular heart disease. For more detailed valvular

analysis, for accurate study of leaflet morphology/mobility before valvular interventions and for reliable diagnosis in doubtful cases a transesophageal echocardiography (TEE) is commonly performed.

Aortic stenosis (AS)
In patients with aortic stenosis (AS), good quality 2D US (TTE) enables assessment of the valve leaflet morphology and mobility and extent of calcification. US based quantification of the functional severity of AS is typically performed by estimating the pressure gradient across the valve. This requires the assessment of the maximal velocity through the stenotic valve using Doppler US and application of the simplified Bernoulli equation. In addition, measurement of the anatomic opening area (planimetry) is performed, and an estimation of the effective valve area is made using the continuity principle. The latter requires measurement of the cross-sectional area of the left ventricular outflow tract for quantification of the left ventricular stroke volume. Due to limitations in the accuracy and image quality of 2D US, in combination with modeling assumptions used in the assessment, the reliability of US based grading of AS severity is sometimes contested. Three-dimensional US has shown to provide more accurate assessment, although this technique has yet to find its place in standard clinical practice. In case of equivocal results from US, invasive pressure gradients obtained during left heart catheterization and the invasive estimation of valve area using the Gorlin formula are commonly used. A non-invasive imaging modality such as cardiac magnetic resonance imaging (CMR) may be used to provide accurate assessment of the aortic valve area and flow across the valve using velocity-encoded CMR. Additionally, cardiac CT (CCT) may be applied to allow quantification of valve calcification and aortic valve area. CCT also provides many relevant anatomical details that are used in planning of percutaneous aortic valve replacement procedures.

Mitral regurgitation (MR)
MR may be the result of degeneration but also a result of (non-)ischemic left heart disease. Surgical mitral valve repair has become the preferred intervention rather than mitral valve replacement, mainly because it preserves the original heart structure, avoiding abnormal remodeling. As such, imaging techniques are applied to determine whether the patient is a suitable candidate for valve repair and to assess all relevant aspects of the valve pathology, being 1) the disease etiology, 2) the primary valve lesion and 3) the resultant valve leaflet dysfunction. TEE is the preferred imaging modality for this advanced mitral valve assessment due to superior exposition of mitral valve complex compared to TTE, and superior dynamic/functional assessment compared to CT/MRI. In the classification system proposed by Carpentier (Carpentier, 1995) for valve leaflet dysfunction three classes are discerned: normal leaflet motion (Type I), excessive leaflet motion (Type II) and restrictive leaflet motion (Type III). Type III can be further divided into restricted leaflet motion as a consequence of rheumatic valve disease (Type IIIa) and restricted leaflet motion due to papillary muscle displacement as a result of (non-)ischemic ventricular dysfunction and dilatation (Type IIIb).

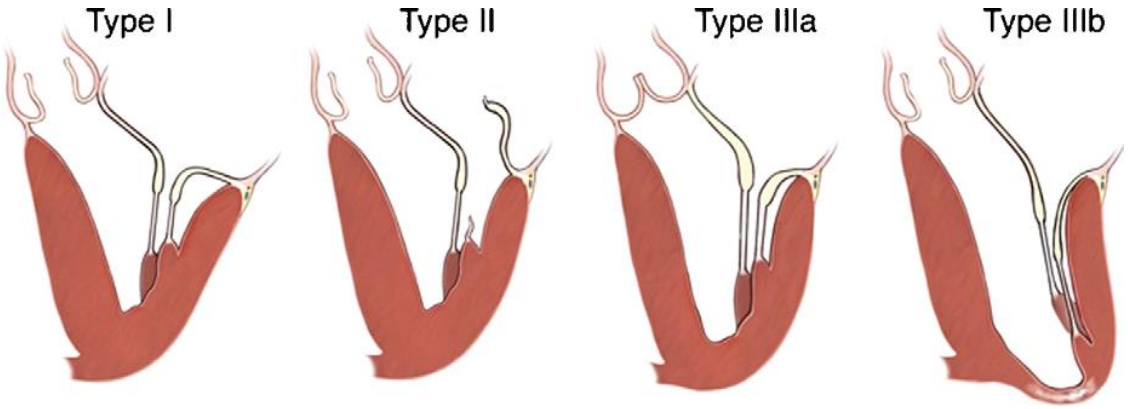

Functional classification of mitral regurgitation according to the classification system of Carpentier. Type I: normal leaflet motion. Type II: increased leaflet motion. Type IIIa: restricted leaflet motion during diastole and systole. Type IIIb: restricted leaflet motion during systole (Chikwe, 2009).

Aortic regurgitation (AR)

The incidence of AR increases with age. AR may result in left ventricular volume overload, but also in increased systolic wall stress which often causes significant eccentric hypertrophy. Patients with severe AR may remain asymptomatic for many years. Patients with AR therefore often require a longer follow-up than those with other forms of VHD. The most important part in patient follow-up is the assessment of LV dimensions and function using standard echocardiography. Several additional imaging modalities may be used such as 3D echocardiography, radionuclide ventriculography or CMR. CMR is particularly useful in AR patients as it allows accurate measurement of LV volumes and function, but also aortic dimensions and calculation of regurgitant volume and fraction.

Mitral stenosis (MS)

The prevalence of MS in developed countries is relatively low because rheumatic heart disease is the primary cause of MS. TTE with Doppler velocimetry is the key diagnostic tool. Planimetry based on TTE images of the mitral valve in mid-diastole is used to quantify the valve orifice. The Bernoulli equation is used to calculate the mean pressure gradient from Doppler velocities, and the pressure half-time method is used to assess the severity of the stenosis from a functional perspective.

Echocardiographic indicators of severe valvular heart disease

Valvular lesion	***Index***	***Threshold for severe abnormality***
Mitral regurgitation	Color Doppler het area Vena contracta width EROA by flow convergence Regurgitant volume Regurgitant fraction Supportive findings	> 40% LA area > 10cm^2 ≥7 mm ≥ 40mm^{2*} ≥ 60 ml ≥ 50% E Wave velocity >1.2 m/s LA or LV dilatation Pulmonary venous flow reversal
Mitral stenosis	Transmitral gradient Mitral valve area Supportive findings	>10 mmHg <1 cm2 PAP > 50 mm HG
Aortic stenosis	Peak aortic velocity Aortic valve mean gradient Aortic valve area	> 4 m/s > 40 mmHg < 1 cm2

	Aortic valve area index Z_{VA}	< 0.6 cm^2/m^2 > 5 mmHg/ml/m^2
Aortic regurgitation	CW Doppler half-time Vena contracta with EROA by flow convergence Regurgitant volume Regurgitant fraction Supportive findings	< 200 ms > 6 mm ≥ 30 mm^2 ≥ 60 ml ≥ 50 % Pan-diastolic flow reversal proximal descending aorta
Each measure should not be taken in isolation but in concert with other signs and imaging parameters to ascertain lesion severity. *An EROA cut-off ≥20 mm2 may have greater sensitivity for severe mitral regurgitation if functional in nature. CW: continuous wave; EROA: effective regurgitant orifice area; LA: left atrial; LV: left ventricular; PAP: pulmonary arterial pressure; Z_{VA}: valvulo-arterial impedance (source Leong 2013).		

4.1.3 State of the art on risk stratification, intervention selection and success evaluation

The most up to date guidelines regarding the management of patients with VHD are described by the Task Force on Practise Guidelines of the American College of Cardiology and the American Heart Association (Nishimura, 2014).
Depending on the type of VHD several qualitative and quantitative indices are used in patient risk stratification, decision making regarding the proper medical intervention and treatment evaluation. The table above provides a list of the most relevant clinically used echocardiographic indices for evaluation of patients with VHD. The indices listed with its associated threshold values are considered a general guideline. The established threshold values should be used with care as for the individual patient valve disease often is not an isolated pathology but may come in combination with other abnormalities such as coronary artery disease, left ventricular hypertrophy, left ventricular dysfunction or other risk factors.
A complicating factor in assessing the severity of VHD is that valve dysfunction is dependent on various factors including loading conditions. Clinical symptoms may only reveal during exercise, which implies that imaging during stress may be required to reveal the true significance of the valve abnormality. The vena contracta width which is used as index in patients with valvular regurgitation has been shown to be less influenced by hemodynamic variables and has previously been shown to correlate with angiographic estimates of regurgitation severity. However, because of the small values of the width of the vena contracta (usually < 1 cm), small errors in its measurement may lead to a large percent error and misclassification of the severity of regurgitation. It is therefore advised to apply an integrative method combining multiple echocardiographic and clinical parameters when grading valvular heart disease. For instance, in patients with AS it has been shown that the prognosis is poor in case of a peak aortic velocity exceeding 4 m/s. However in patients with depressed LV function and thus low forward flow severe AR may be present with lower peak aortic velocity. In those circumstances it is important to also assess the aortic valve area and stroke volume. Invasive pressure measurements during cardiac catheterization may also be required.

In asymptomatic patients for whom the severity of the VHD does not yet require interventional treatment frequent monitoring is required. Imaging during follow-up visits should include assessment of the hemodynamic severity of the diseased valve, but also assessment of left ventricular and atrial dimensions.

We will describe the treatment options for aortic stenosis and mitral valve regurgitation, as they represent the majority of the cases.

Aortic valve stenosis

The figure below schematically presents the current recommended clinical indications for aortic valve replacement in patients with AS. Evaluation of the success of the interventional treatment is primarily based on assessment of the pressure gradient across the valve based on echocardiography. In patients undergoing TAVI invasive pressure measurements are obtained under X-ray fluoroscopy. Surgical aortic valve replacement has been the standard of care in patients with severe symptomatic aortic stenosis. However, elderly patients can be at high risk for a surgical aortic valve replacement because of frailty and comorbidities. Therefore, next to classical surgical treatments (surgical replacement, minimally invasive surgical replacement, apicoaortic conduit) the transcatheter aortic valve implantation (TAVI) is expanding. TAVI has become a clinical option only less than a decade ago and it is already the standard treatment for inoperable patients. Technological progress is improving the outcome of TAVI, resulting in gradually expanding the target population (Makkar, 2014) (Osnabrugge, 2015).

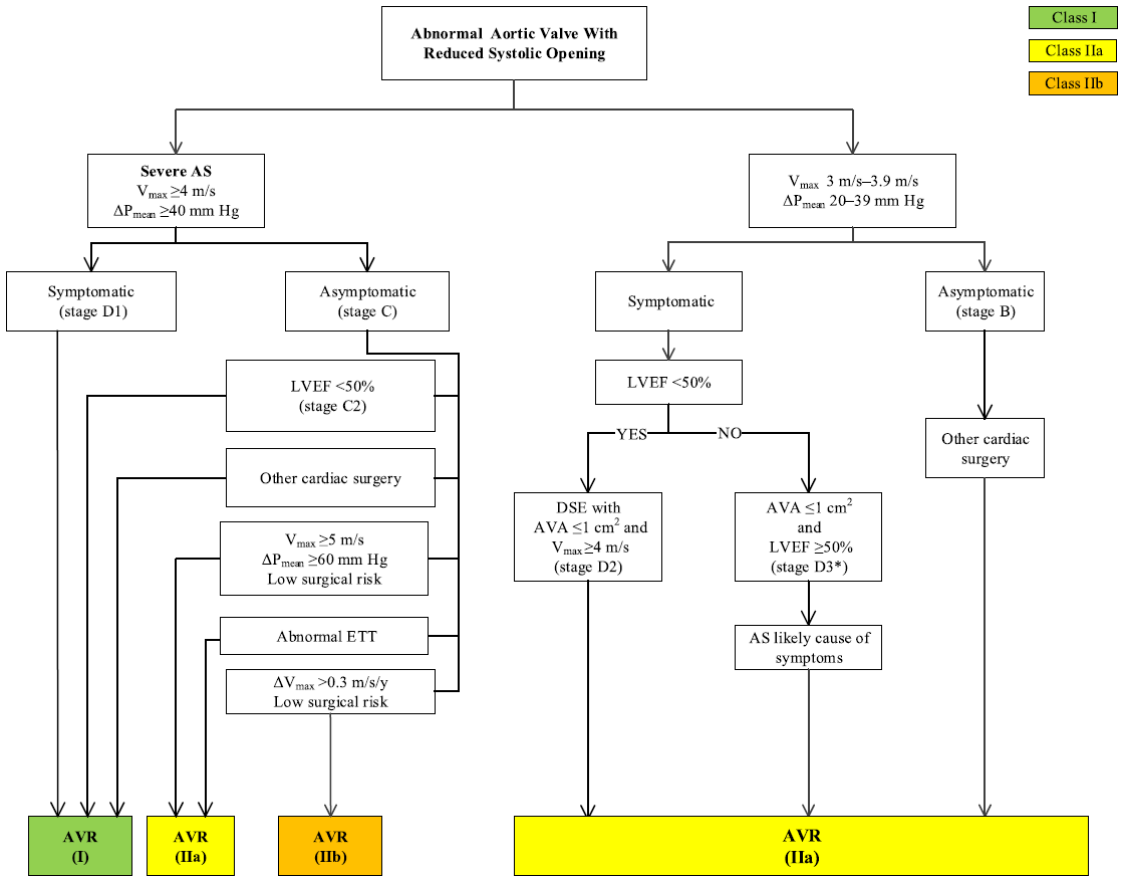

Indications for aortic valve replacement in patients with aortic stenosis

Arrows show the decision pathways that result in a recommendation for AVR. Periodic monitoring is indicated for all patients in whom AVR is not yet indicated, including those with asymptomatic AS (stage D or C) and those with low-gradient AS (stage D2 or D3) who do not meet the criteria for intervention.
**AVR should be considered with stage D3 AS only if valve obstruction is the most likely cause of symptoms, stroke volume index is <35 mL/m2, indexed AVA is ≤0.6 cm2/m2, and data are recorded when the patient is normotensive (systolic BP <140 mm Hg).*
AS: indicates aortic stenosis; AVA: aortic valve area; AVR: aortic valve replacement by either surgical or transcatheter approach; BP: blood pressure; DSE: dobutamine stress echocardiography; ETT: exercise treadmill test; LVEF: left ventricular ejection fraction; DPmean: mean pressure gradient; Vmax: maximum velocity. (Nishimura, 2014)

Mitral valve regurgitation

When pharmaceutical treatment is not sufficient the mitral valve regurgitation may require an intervention to repair or replace the valve. The figure below schematically presents the current recommended clinical indications for mitral valve repair or replacement. Classical treatment requires invasive surgical intervention: replace the valve with a (bio)-prosthetic device or repair the valve, e.g. by adding a ring (ring annuloplasty) or by stitching the two leaflet edges (edge-to-edge technique or Alfieri stich). More recently, minimally invasive and even percutaneous trans-catheter interventions are emerging, replicating surgical options. For the moment, there is only one device for transcatheter mitral valve repair recommended for clinical use, being the MitraClip (Glower, 2014). The latter device replicates the edge-to-edge technique using a transcatheter approach. However, other devices are undergoing clinical trials both for repair and replacement. The success of the intervention treatment is primarily based on echocardiography, i.e. by assessment of the residual regurgitation.

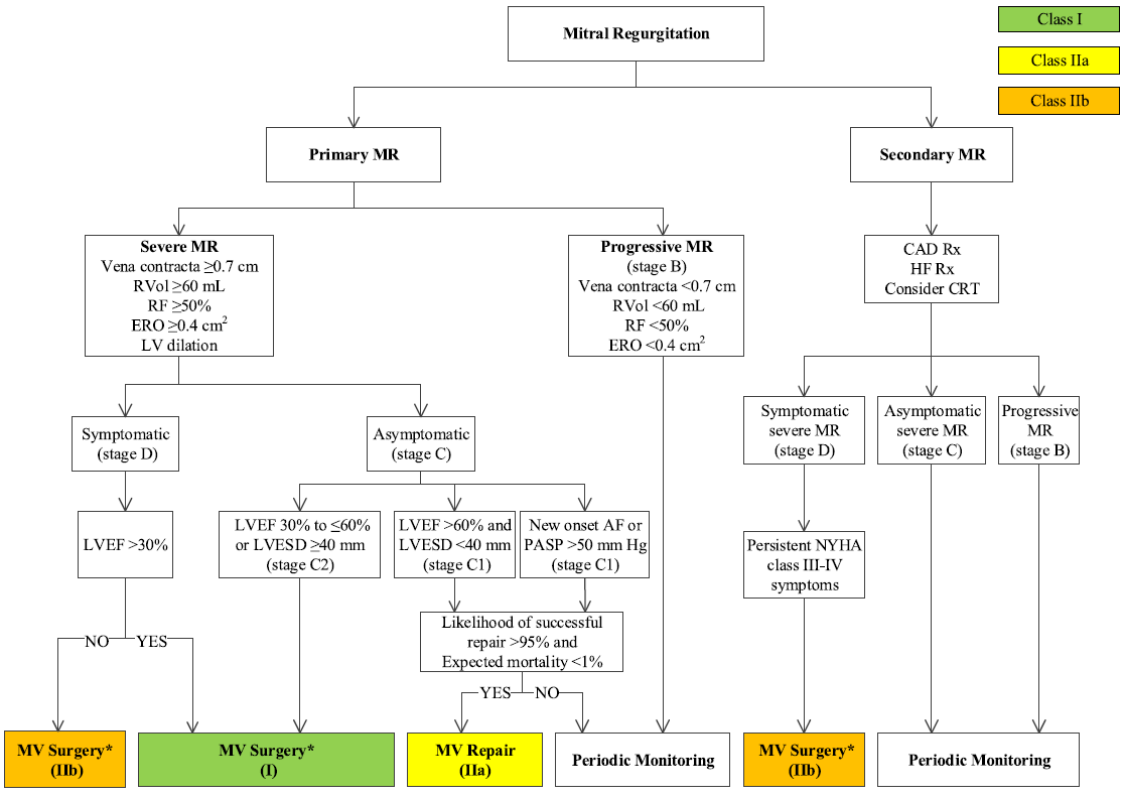

Indications for surgery in patients with MR.

AF: atrial fibrillation; CAD: coronary artery disease; CR:, cardiac resynchronization therapy; ERO: effective regurgitant orifice; HF: heart failure; LV: left ventricular; LVEF: left ventricular ejection fraction; LVESD: left ventricular end-systolic dimension; MR: mitral regurgitation, MV: mitral valve; MVR: mitral valve replacement; NYHA: New York Heart Association; PASP: pulmonary artery systolic pressure; RF: regurgitant fraction; RVol: regurgitant volume; Rx: therapy. (Nishimura, 2014)

4.1.4 BENEFIT updates

TAVIguide: engineering simulations to optimize Transcatheter Aortic Valve Replacement

FEops has developed a simulation-based technology to predict the outcome and the complications of transcatheter aortic valve replacement starting form routine preoperative imaging.

To virtually treat a patient's heart using TAVIguide, the doctor has to upload the CT image (anonymized DICOM file) through a secured web portal. After 24 hours, the doctor receives the simulation results from FEops on the same portal and can visualize the virtual patient treated using different (possible) procedural options. For each procedure, the 3D model of heart and device can be inspected by rotating / translating and zooming, thanks to the webGL technology. In addition to the 3D models, contour plots and measurements are provided that describe specific physical quantities corresponding to the onset of treatment complications. For the paravalvular leak, blood flow streamlines colored by velocity are shown around the device and the amount of regurgitating flow is reported (fluid flow, in ml/min). Similarly, the risk of conduction abnormality is indicated by contact pressure (distribution and value) exerted by the device onto a region of the heart where the conduction system is located (and can be damaged!). In this way, the doctor can compare the simulated outcome of multiple possible procedural options and is optimally informed to deliver the optimal treatment to the patient.

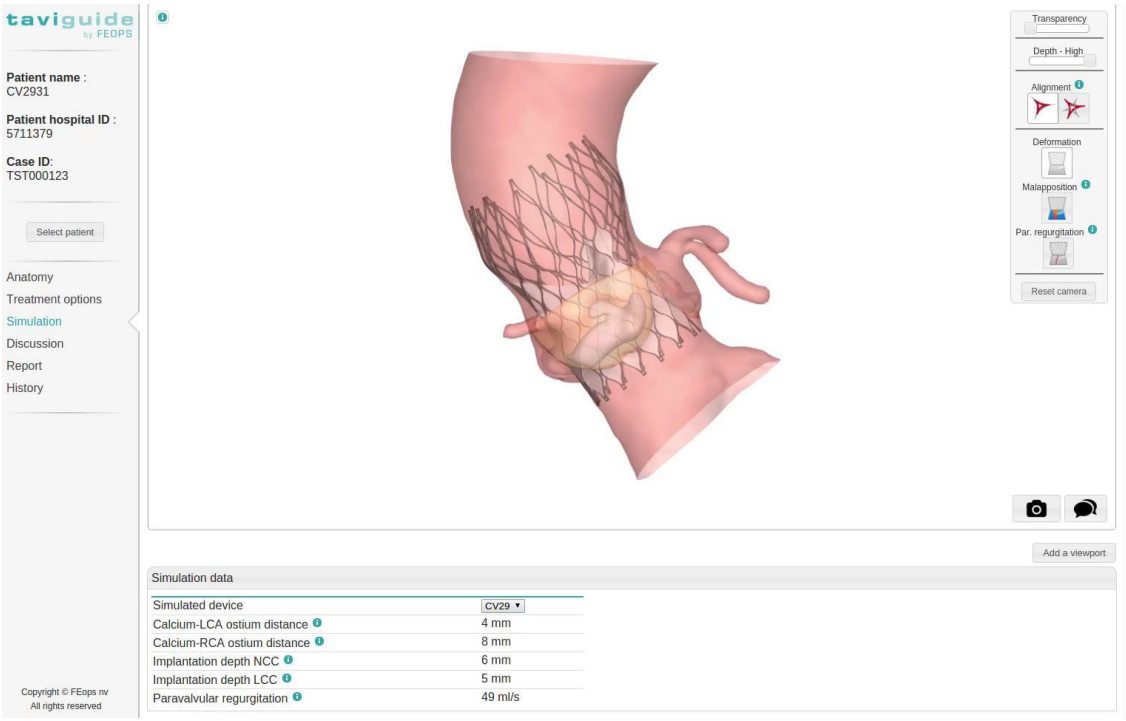

The final doctor's evaluation is needed because the optimal treatment is often a compromise to avoid (or lower) the risk of multiple complications (i.e. a trade-off).

From a technical point of view, TAVIguide combines state-of-the art segmentation, to reconstruct a patient's unique anatomy, and simulations, to simulate the expansion of the device in a patient's heart (using Finite Element Analysis) and to simulate the blood flow after TAVI (using Computational Fluid Dynamics). On top of that, TAVIguide requires a database of computer models of existing TAVI devices, and clinical investigation to calibrate the simulation settings (e.g. stiffness of different regions of the heart) and to relate the risk of complications to physical quantities that can be measurable from the simulation results.

TAVIguide is currently being evaluated clinically in a prospective multicenter study. Until now, two retrospective investigations have shown the potential of TAVIguide in predicting the outcome of TAVI procedures and have resulted in 2 scientific publications.

The clear advantage of TAVIguide is that complications can be evaluated upfront and, therefore, avoided during treatment, potentially increasing the life-expectancy of the patient after TAVI. By complementing the current treatment planning (usually based on anatomical measurements only), engineering simulations have the potential to go beyond TAVI and support multiple emerging structural heart interventions, such as transcatheter closure of left atrial appendage, repair and replacement of mitral and tricuspid valves and treatment of heart failure.

<u>LUMC: 4D flow imaging and analysis</u>
Methods have been developed and software tools implemented for cardiac valve evaluation based on MR imaging. An MR imaging protocol has been developed for imaging the dynamic 3D velocity field within the heart over the complete cardiac cycle.

The spatial resolution of the 4D flow acquisition is ~ 3×3×3 mm3, which has shown to be sufficient for assessment of the large-scale flow structures within the heart. The temporal resolution obtained is ~40ms, resulting in ~30 phases across the complete cardiac cycle. The reliability of the developed 4D flow imaging sequence was compared to two other alternative 4D flow sequences. Compared to the other sequences, the proposed sequence demonstrated the least susceptibility artifacts, good image quality and the highest consistency of intra-cardiac flow quantifications. The results of this study have been published in (Garg, 2017). In addition to the 4D flow scan, the imaging protocol includes multiple cine acquisitions using standardized cardiac views allowing accurate assessment of the ventricular morphology throughout the cardiac cycle. For quantitative and visual analysis of the intra-cardiac blood flow, particle tracing techniques have been developed allowing studying the dynamic patterns of intra-cardiac blood flow in high detail. The result of particle tracing is converted into VTK format, facilitating 3D visualization of the results using available software tools. For quantitative analysis, the particle tracing results are used as input to perform multi-component flow analysis. Using this technique, the intra-cardiac blood flow is classified into the following five categories based on the blood flow trajectory of a particle within a single cardiac heart beat: 1) *retained inflow*, 2) *delayed ejection*, 3) *direct flow*, 4) *residual volume* and 5) *valvular regurgitation*. For this analysis, first, the left ventricular cavity is segmented in the end-diastolic (ED) and end-systolic (ES) phases using the short-axis multi-slice cine scan. The LV cavity at ED is used to define synthetic particles that are traced forward and backward in time using the 3D velocity field from the 4D Flow scan.

Several imaging artifacts may impact the accuracy of the particle tracing analysis. Spatial mis-registration between the short-axis cine scan and the 4D Flow scan will result in inaccurately defined blood particles. An automated image registration method was developed to minimize the amount of mis-registration. Another potential source of error is the presence of velocity offset errors in the 4D Flow image data. An offset correction method was developed based on the assumption of static myocardial tissue at the moment of ED and ES. Validation of the correction method has been performed in a scan-rescan setting. The results of this study indicate that both correction methods improve the reliability of the particle tracing results (Kamphuis, 2017).

The result of image segmentation and intra-cardiac flow analysis can be used as input for pre-procedural planning of valvular interventions using approaches as developed by Feops. The 3D+time geometrical models from MRI data can be used by Feops for pre-operative planning of patients undergoing a mitral valve intervention.

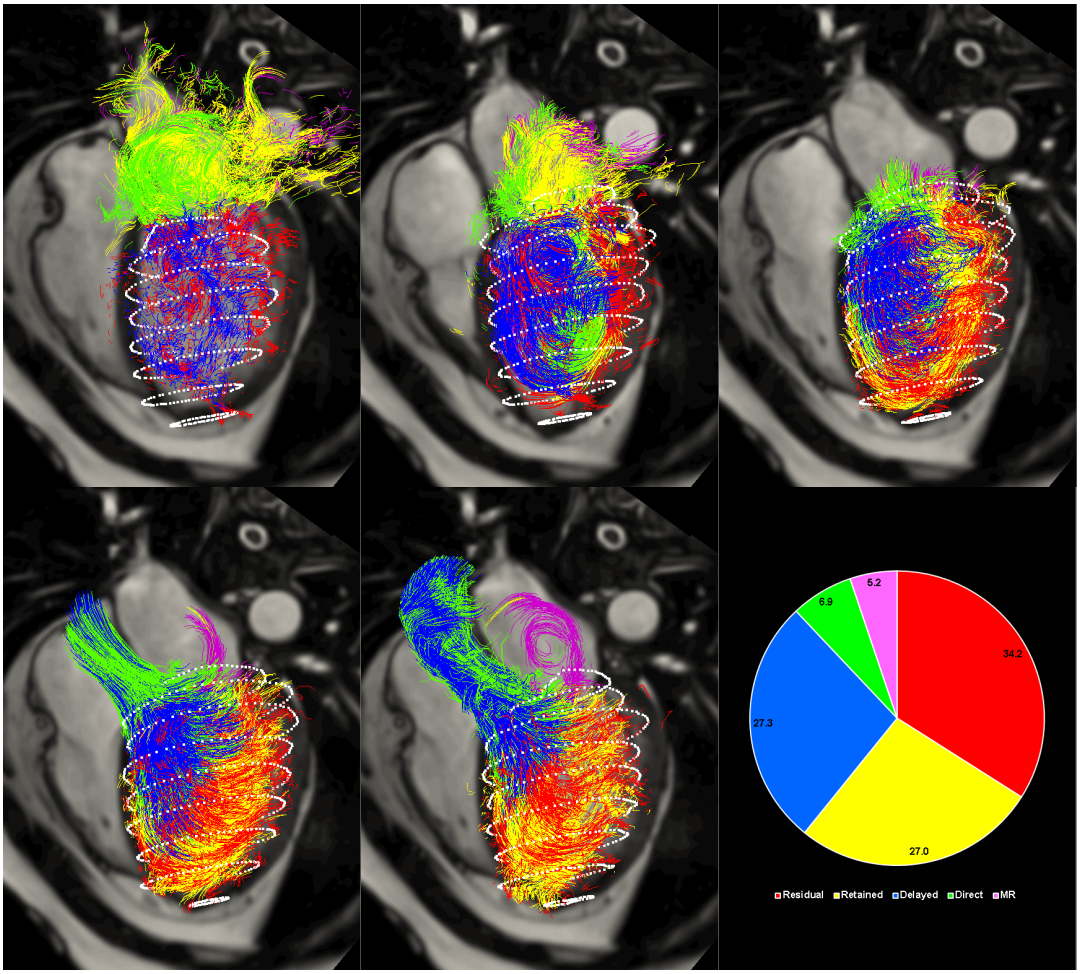

Result of left ventricular flow-component analysis using particle tracing from 4D Flow MRI. The trajectory of blood particles is computed over a complete cardiac cycle and classified for each particle according to the followed trajectory through the LV cavity and the mitral and aortic valve planes. Particle traces are shown for 5 consecutive time points within the cardiac cycle. The pie chart displays the relative number of particles for each of the 5 defined categories.

For quantification of arterial stiffness based on MR imaging, an automated image segmentation and blood flow velocity quantification method has been developed. The pulse wave velocity (PWV) – the propagation speed of the pressure wave through the artery – is a validated biomarker for arterial stiffness. With MRI the PWV can be assessed using a combination of anatomical imaging to assess the length of a vessel segment and the use of high temporal resolution phase-contrast MRI to assess the blood flow velocity at multiple vessel cross-sectional positions. An automated method was developed for 3D segmentation of the aortic arch in a stack of anatomical images using a multi-atlas registration approach. From this the length of the aorta centerline can be derived. Further, using the centerline, seed points in the aortic lumen can be derived, allowing fully automated aorta segmentation in phase-contrast scans at various aorta cross-sections. The combination of the two developed techniques allows fully automated quantification of PWV of the aortic arch. Using MRI data of 212 patients from four clinical centers the automated analysis pipeline was compared to conventional manual analysis of PWV. The precision of automate aortic length estimation was better than the inter-observer variability of manual measurements and the correlation between manual and automated PWV assessment was shown to be

0.98, indicating excellent performance of the developed automated method. An abstract (Shahzad, 2018) has been submitted which will be presented at the upcoming conference of the Society of Cardiovascular Magnetic Resonance in Barcelona 2018. The results of the evaluation study will soon be submitted as publication for a clinical journal.

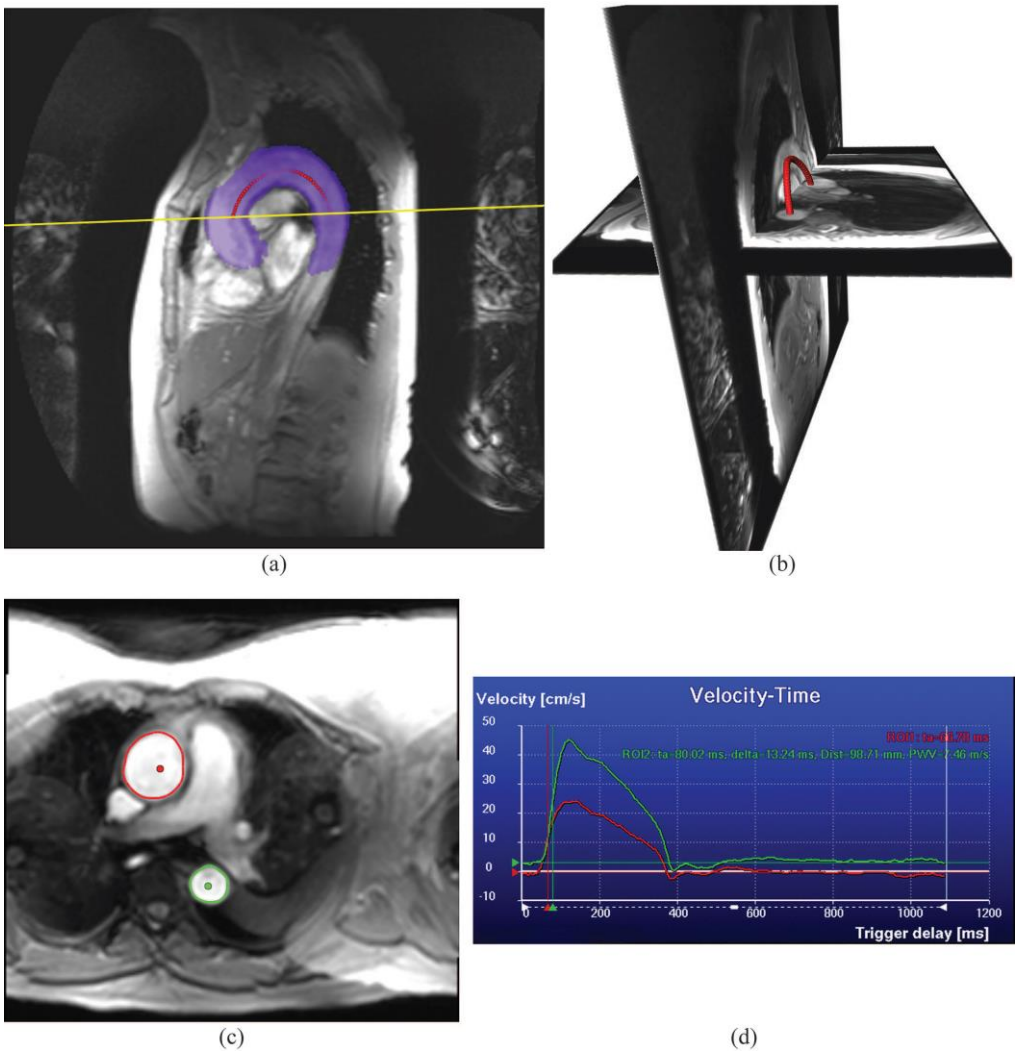

Result of automated image segmentation for pulse wave velocity (PWV) quantification. The 3D centerline (shown in red in a and b) of the aorta is used to compute the length of the aortic arch. The intersection of the centerline with the 2D velocity encoded scan (shown in c) is used a seed point for automated vessel boundary detection. From the flow velocity curve (shown in c) the difference in arrival time of the flow waves is derived in order to compute the PWV.

4.2 Percutaneous Coronary Interventions

Lead author: LUMC

4.2.1 Introduction

Coronary arteries are the blood vessels that take care of the blood supply to the heart muscle. Coronary artery disease is the major cause of death in the Western world (WHO, 2014). The main cause of this disease is atherosclerosis, i.e. a thickening of the coronary artery vessel wall. This process of build-up of fatty deposits in the vessel wall may already start in young adulthood, and continue afterwards. The continued build-up of these plaques may eventually lead to a narrowing or occlusion of the coronary lumen, causing ischemia (lack of blood supply) and angina (chest pain) symptoms. Alternatively, a coronary plaque may rupture and release its contents in the artery, causing blood clots and a sudden occlusion, potentially leading to an acute myocardial infarction (heart attack).
There are several risk factors associated with the development of premature ischemic heart disease and acute myocardial infarction, such as smoking, age, diabetes, hypertension and obesity.

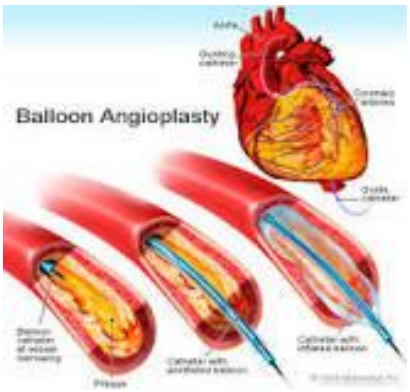

Percutaneous coronary intervention (PCI) is one of the treatment options for patients with chronic stable angina (chest pain due to ischemia of the heart muscle). Other options are medication, and coronary artery bypass graft (CABG). Whereas PCI is less invasive than CABG, and thus seems favorable for patients, the preferred treatment depends on various issues, such as patient characteristics and classification of a lesion, and is still subject to investigations and debate. The interventions do not cure the underlying cause of the atherosclerotic disease process but they are carried out to alleviate the symptoms and have a survival benefit for the patients. For acute patients, CABG and PCI are associated with significant short- and long-term mortality benefit.

Diagnostic preoperative imaging of patients with cardiac problems involves X-ray angiography, which visualizes the lumen of coronary arteries. In this procedure, contrast agent is introduced in the left or right coronary artery, by advancing a catheter via the radial or femoral arteries to the aorta into the coronary ostium. X-ray angiography allows the quantitative assessment of the narrowing of the coronary lumen (stenosis). Coronary X-ray angiography currently is the standard modality for assessing coronary lesions, and a vessel diameter of 50% or less (75% area) is considered a significant lesion. However, the hemodynamic significance of a coronary lesion does not correlate well with stenosis measurements. Therefore other quantitative measurements and imaging techniques, both before the intervention (CTA, SPECT, perfusion MRI, stress echo) and during the intervention (FFR, OCT, IVUS), are nowadays investigated and employed to decide whether a lesion needs treatment. These modalities provide also additional information about the plaque burden and the plaque composition.

4.2.2 Clinical State of the Art

The purpose of PCI is to restore the vascularization of the heart muscle by widening stenotic lesions in coronary arteries. To this end, a stent is placed in the coronary artery, possibly after prior dilation with a balloon. The procedure is performed

minimally invasively, often via the femoral artery (but also via brachial or radial artery). First a guide catheter is introduced, such that the distal tip of the guide catheter is in coronary artery, to provide a safe access of the guide wires and catheters to the coronary arteries. Subsequently, a guide wire is inserted through this catheter, and advanced beyond the lesion. Optionally, additional intravascular imaging or measurements (IVUS/OCT/CFR/FFR) may be performed to assess the hemodynamic significance of the lesion or the burden and composition of the plaque. In case dilation of the lesion before stent placement is needed, a balloon catheter is advanced over the guide wire, positioned at the lesion spot in the coronary artery and inflated to dilate the artery. After dilation, a catheter with a balloon-mounted stent is advanced over the guide wire. When the stent is located at the lesion spot, the balloon is inflated to deploy the stent. After stent deployment, the balloon catheter is removed.

Image guidance during the procedure is performed by mono- or biplane fluoroscopy (see Figure 1), which visualizes the guide wires and catheters (some of which have additional markers for improved visibility). The coronary arteries are visualized by injections of contrast agent, which result in a transient visualization of the vessels. Optionally after the stent placements, the stent deployment is checked by using IVUS or OCT. If struts are not positioned correctly against the lumen wall, a second balloon inflation might be needed to place the struts correctly for a better end result of the procedure.

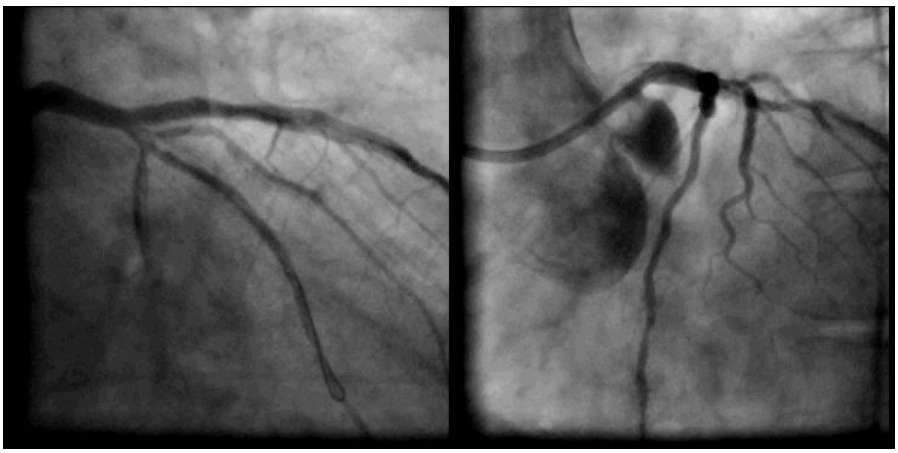

Figure 1: Biplane image of coronary intervention (Image courtesy Erasmus MC)

4.2.3 State of the art on risk stratification, intervention selection and success evaluation

In case of chronic (not acute) complaints, the following diagnostic means can be used for patient stratification:

- Patient complaints and history, including risk factors such as age, gender, diabetes, blood cholesterol level, smoking habit, blood pressure, medication, previous interventions and family history
- Heart sounds (stethoscope)
- ECG recording during rest and stress in a clinical situation (e.g. the bicycle test) or for a longer time (1 day to 2 weeks) during normal activity with a wearable Holter monitor.

- CT Angiography from which several values can be deduced such as vessel sizes and obstructions, coronary artery calcium score, ejection fraction, TIMI flow and virtual FFR
- Cardiac ultrasound to determine the heart contraction pattern, ejection fraction and blood flow under normal and stress condition
- Cardiac PET scan to determine viability of the heart tissue.

Some of these risk factors have been combined in composite scores, such as the Framingham risk score and the Syntax score (Farooq, 2013). Professional societies have composed guidelines to use risk factors for choice of treatment and follow up, see figure below (Windecker, 2015) which may also partly depend on national or local circumstances (such as availability of equipment and payment by insurance companies)..

Risk models to assess medium- to long-term (≥1 year) outcomes

Score	Development cohort	Patient inclusion	Coronary procedures	Number of variables		Outcome	Recommendation		Validation studies	Calculation	Ref[a]
				Clinical	Anatomical		CABG	PCI			
SYNTAX	None, expert opinion	none	-	0	11 (3 general, 8 per lesion)	MACCE	I B	I B	>50	www.syntaxscore.com	30
SYNTAX II	1800 Multicentre	03/2005 – 04/2007	50% CABG, 50% PCI	6	12	4-year mortality	IIa B	IIa B	<5	-	25
ASCERT CABG	174 506 Multicentre	01/2002 – 12/2007	100% (i) CABG	23	2	Mortality >2 years	IIa B		<5	-	27
ASCERT PCI	206 081 Multicentre	2004 – 2007	100% PCI	17	2	Mortality >1 year		IIa B	<5	-	28
Logistic Clinical SYNTAX	6 508 Multicentre	03/2005 – 04-2007	100% PCI	3	11	1-year MACE and mortality		IIa B	<5	-	24

ASCERT: American College of Cardiology Foundation–Society of Thoracic Surgeons Database Collaboration (ACCF–STS) on the comparative effectiveness of revascularization strategies; (i) CABG: (isolated) coronary artery bypass grafting; MACCE: major adverse cardiac and cerebrovascular events; PCI: percutaneous coronary intervention; SYNTAX: synergy between percutaneous coronary intervention with TAXUS and cardiac surgery.

Treatment choices are:
- No direct need for medication or intervention
- Medication only (for instance cholesterol or blood pressure lowering drugs)
- PCI: minimally invasive intervention via a catheter to remove a vessel obstruction
- Coronary Artery Bypass Graft (CABG) surgery: surgical creation of a bypass for the obstructed vessel(s) using a part of a vessel from another part in the body.

Acute patients will mostly be sent directly to the intervention room (with premedication) for coronary angiography to assess the condition of the vessels and heart function and if necessary immediately restore vessel diameter and blood flow to the under-perfused parts of the heart.

Several qualitative and quantitative measurements can be made during the intervention:
- Measurement of vessel diameter in ‘normal’ and partly obstructed segments (QCA, Quantitatve Coronary Analysis),
- Perfusion of the tissue behind a vessel branch (TIMI flow)

- Fractional Flow Reserve (FFR) or instantaneous wave free ratio (iFR) (Petraco, 2014) indicating the functional severity of a vessel obstruction, using a dedicated pressure wire

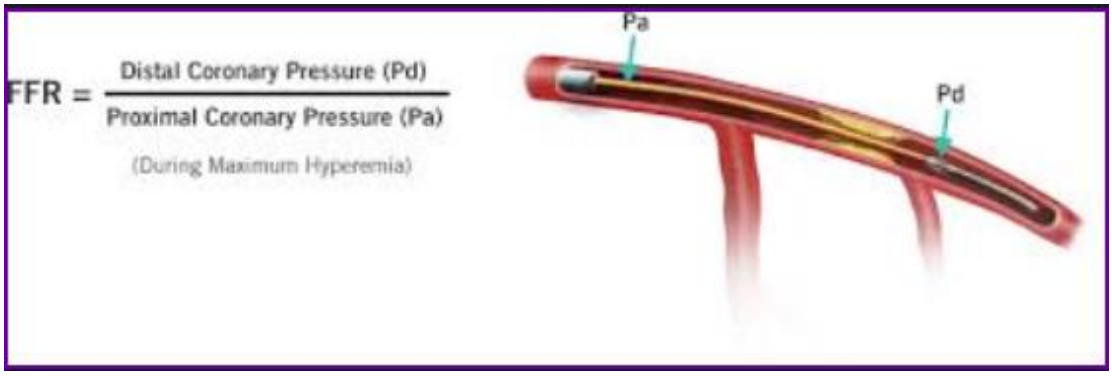

- Index of Microcirculatory Resistance with a pressure-temperature wire (Fearon, 2013)
- Intra-arterial imaging with US or OCT to assess the vessel wall condition and to characterize the obstructing tissue (plaque)

Determination of success during and directly after an intervention is mostly based on visual assessment of vessel diameter and blood flow before and after the procedure. Short term success can also be quantified in lumen diameter before and after the intervention, FFR and peri-procedural complications.

Longer term success is expressed in long term vessel patency and need for revascularization, MACE (Major Adverse Cardiac Event, such as a heart attack) and death.

4.2.4 BENEFIT updates

Quantitative Flow Ratio
Medis has developed a method for the determination of the so-called “QFR” value, which is a value similar to the FFR measurement, but obtained from 3D model and the input flow velocity of the artery of interest recognized from two 2D X-ray images.

To obtain a 3D model of the coronary artery from biplane X-ray imaging, a 3D centerline is defined as the curve that passes through the center of the vessel lumen. The accuracy of the centerline reconstruction depends both on the 2D centerline extraction and on the 3D point reconstruction. In our approach, 2D contours are automatically detected by a validated contour detection algorithm. 2D centerlines are then extracted from the contours and used to reconstruct the 3D centerline points. The 3D point reconstruction algorithm requires knowledge of the correspondence between the frontal and lateral centerlines.

Further, the volumetric flow rate through the vessel needs to be determined. For this, the contrast medium transport time in the reconstructed vessel is calculated on hyperemic projections using TIMI frame count. The mean volumetric flow rate at

hyperemia was derived using the lumen volume of the reconstructed coronary tree divided by the mean transport time.

From these to inputs (3D vessel model and the hyperemic flow rate), the computation of the QFR can be done. The reconstructed geometry is discretized with tetrahedral cells (meshing), and the Navier-Stokes equations are solved simultaneously. After this, QFR is defined as the mean pressure at the outlet divided by the mean pressure at the inlet. This whole calculation can be done within 1-2 minutes time, which is sufficiently fast to include it in the cathlab workflow.

The QFR is currently being evaluated clinically. A first study that demonstrated its principles was published in 2014 in the JACC Interventions Journal. The outcome showed a very small difference between the QFR- and the FFR-values. In October of 2016 the results of a FAVOR II Pilot Study were published in JACC Interventions. The outcome of this study demonstrated that reliable results can also be obtained without pharmacologic hyperemia induction by adenosine, which bears the potential for a wider adoption of the QFR-based lesion assessment.

The clear advantage of The QFR approach, compared to the current state of the art (FFR) is the fact that no interventional device (like the pressure wire) is needed to obtain the FFR value representing the functional significance of a stenosis. Obsoleting this interventional measurement shortens the procedure, it lowers the inevitable risk for the patient that interventional devices carry, and it is easier to apply to multiple stenoses or diffused vessels.

Further advantage is the fact that the QFR measurement can easily be repeated post-intervention, which means that the improved functional performance after treatment can be shown while the patient is still on the table. If not enough improvement gain to the patient's condition can be shown, further treatment can be initiated immediately. This avoids the patient to have to come back to the intervention room at a later stage.

Automatic detection of stent struts by OCT imaging

If stent struts are not directly apposed to the blood vessel wall there is an increased risk that the vessel will get occluded again due to stent thrombosis. Manually checking of the position of the struts is too time consuming so in BENEFIT a procedure has been developed for automatic recognition of the struts and the vessel wall and to determine the fraction of struts that are 'malapposed'. This was compared with manual detection by an expert and the overlap between both methods was quantified by the so called dice index. Struts were considered similar when the dices index is above 80%

In a cohort of 8 patients with almost 8000 struts, the average score of true positives was 89.8%, 8.8% for false positives and 8.3% for false negatives. The F score was 91.6. (Liu, 2016). This was a population especially also with imaging artefacts.

The table below shows the stent struts detection results

Data set	No. of GT	Original Pullback (%)				Compensated Pullback (%)			
		TP	FP	FN	*F*-score	TP	FP	FN	*F*-score
1	776	86.5	21.4	13.5	83.2	89.4	19.8	10.6	**85.5**
2	891	94.2	8.5	5.8	92.9	96.1	9.1	3.9	**93.7**
3	1158	82.6	2.7	17.4	**89.1**	79.6	3.7	20.4	86.9
4	910	78.2	1.4	21.8	87.1	89.2	1.5	10.8	**93.5**
5	1389	91.9	8.9	8.1	91.5	95.1	7.9	4.9	**93.7**
6	847	85.0	22.8	15.0	81.8	88.7	14.3	11.3	**87.4**
7	1059	81.7	17.2	3.6	88.7	81.8	13.1	3.5	**90.8**
8	903	96.6	4.3	3.4	**96.1**	96.6	5.5	3.4	95.6
Total	7933	87.2	10.4	10.9	89.1	89.5	9.0	8.6	**91.0**

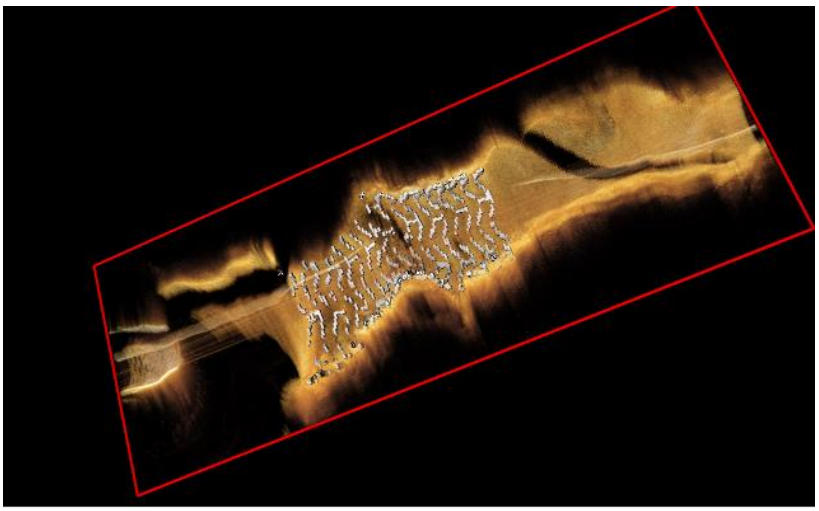

3D visualization of detected struts.

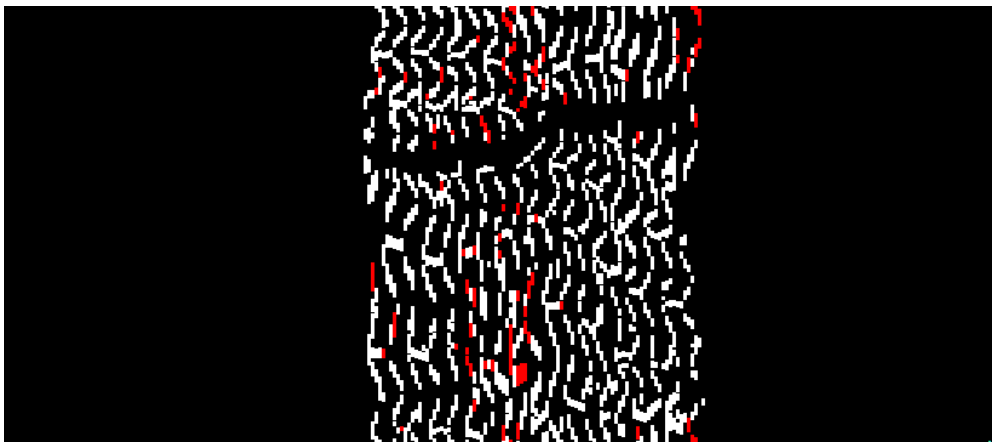

2D “fold-out” map with malapposed struts indicated in red.

4.3 Brain vessel interventions

Lead authors: EMC

4.3.1 Introduction

The use case of brain vessel interventions will focus on intracranial aneurysms. An intracranial aneurysm (also called cerebral or brain aneurysm) is a cerebrovascular (related to brain vessels) disorder in which weakness in the wall of a cerebral artery or vein causes a localized dilation or ballooning of the blood vessel. Intracranial aneuryms are quite common, with frequencies report from 0.5 to 9 % (based on imaging and autopsy studies).
The main risk of intracranial aneurysms is a rupture, and a subsequent bleeding (subarachnoid hemorrhage) (Loewenstein, 2012). The majority (~ 80%) of such bleedings in the brain that do not result from trauma, are caused by an aneurysm rupture. These bleedings are associated with 1-month mortality rates ranging from 30% to 50%. Additionally, patients surviving these bleedings may have neurological or functional problems because of the bleeding, or because of rebleeding and insufficient blood supply to the brain. A rupture thus has very serious consequences, and therefore, accurate risk assessment for rupture prediction is of crucial clinical importance.

Cerebral aneurysms are classified both by size and shape. Small aneurysms have a diameter of less than 15mm. Larger aneurysms include those classified as large (15 to 25mm), giant (25 to 50mm), and super giant (over 50mm). A small, unchanging aneurysm will produce few, if any, symptoms. Indeed, many aneurysms are unnoticed, and are discovered incidentally. Also, ruptures can come without clinical symptoms, though before a larger aneurysm ruptures, the individual may experience symptoms as a sudden and unusually severe headache, nausea, vision impairment, vomiting, and loss of consciousness, or the individual may be asymptomatic (i.e., experiencing no symptoms at all).

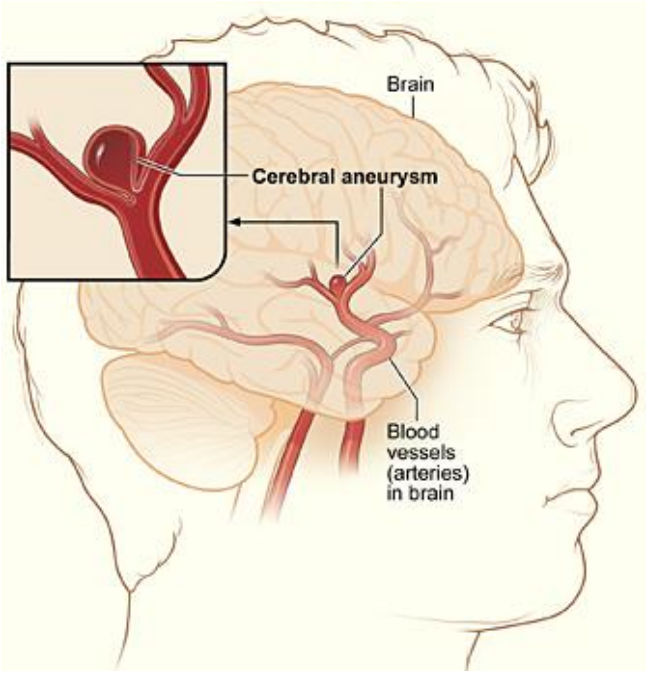

Intracranial Aneurysm (source: Wikipedia)

4.3.2 Clinical State of the Art

When an intervention is deemed necessary (because rupture risk exceeds risks associated with the intervention, or when the aneurysm already ruptured), there are two main types of treatments: neuro-surgical intervention, e.g. clipping of the aneurysm, and endovascular interventions, such as coiling (with or without stent-

assistance) and flow diverters. All of the interventions are focused on preventing blood flow into the aneurysm, thus stimulating clot formation, thus reducing the pressure on the aneurysm wall, and reducing rupture risk or rebleeding.
Surgical clipping is the traditional option for treatment of large aneurysms. Clipping was first perfomed in 1937. In this neuro-surgical procedure, a metal clip, specifically chosen for the aneurysm, is put at the neck of the aneurysm, thus excluding it from blood circulation. This procedure is highly effective, but associated with risks due to the nature of open surgery. It also has been shown that postoperative outcomes depend on the expertise and experience of the neurosurgical team. Neuro-surgical interventions are outside the scope of the project, and will not be discussed further.

Endovascular coiling is a minimally invasive intervention that has been introduced around 20 years ago. In this intervention, catheters are maneuvered to the location of the aneurysm, and subsequently several metal coils are brought into the aneurysm. These coils minimize blood flow and stimulate clot formation.

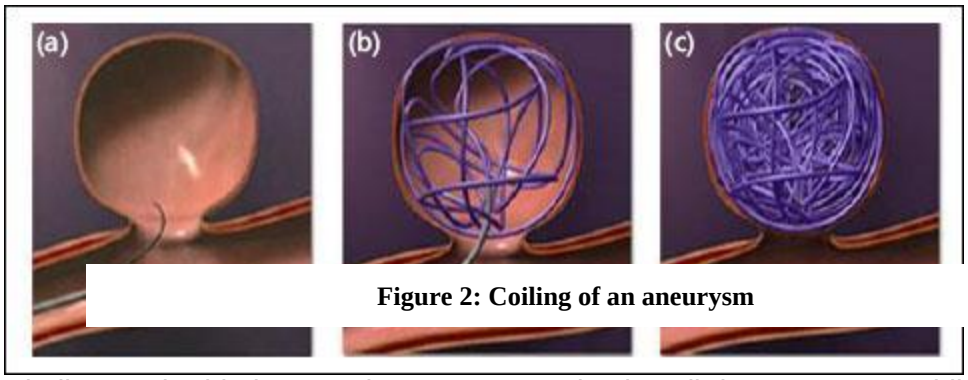

Figure 2: Coiling of an aneurysm

Challenges in this intervention are to completely coil the aneurysm, while preventing coils entering the feeding vessels. Accurate assessment of aneurysm size and morphology is relevant for these interventions. The main risks associated with clipping are the formation of clots or rebleeding.

Recently, several more advanced approaches have been introduced for the endovascular treatment of intracranial aneurysms, such as stent-assisted techniques and flow diverters. The stent-assisted coil embolization technique has broadened the field for endovascular treatment of intracranial aneurysms to wide-neck aneurysms. The use of neurovascular stents that serve as a scaffold allows for higher coil packing densities with a relatively low chance of coils herniating into parent arteries. Currently, its application is not limited only to giant and fusiform aneurysms but it is also being used for smaller berrylike aneurysms.

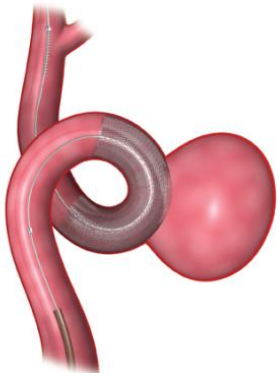

Aneurysm treament by flow diverter

4.3.3 State of the art on risk stratification, intervention selection and success evaluation

Rupture risk prediction, as stated before, is crucial for clinical decision making in the case of unruptured intracranial aneurysms. However, despite many studies investigating rupture risks, a clear decision model is still lacking.
Intracranial aneurysms may result from diseases acquired during life, or from genetic conditions. Lifestyle diseases including hypertension, smoking, excess alcohol consumption, and obesity are associated with the development of aneurysms. Other acquired associations with intracranial aneurysms include head trauma and infections.
Several studies have looked at other identifiying factors for rupture risk. Size of the aneurysm has been shown to be a significant predictor for rupture. However, a clear cut-off threshold above which aneurysms have a (much) greater risk is not known, nor is the exact relation between aneurysm size and rupture risk
Aneurysm growth also is also hypothesized to be a predictor for rupture risk. Additionally, aneurysm growth leads to larger aneurysms, which in themselves also are associated with larger rupture risks.
Aneurysms in the posterior circulation (basilar, vertebral and posterior communicating arteries) also have a higher risk of rupture. Basilar artery aneurysms represent only 3%-5% of all intracranial aneurysms but are the most common aneurysms in the posterior circulation.
The relation between rupture risk and aneurysm morphology has also been investigated. Aneurysm-to-vessel size ratio, and aneurysm angle have strong correlation with rupture risk. Other paramaters that have been demonstrated to correlate with rupture risk are the deviation of the shape from a sphere and the number of concave regions on the aneurysm surface.

Despite all these studies, there are no hard criteria on which a decision on treatment can be based. The current guidelines (Steiner, 2013) still suggest that the decision should be based on a multidisciplinary discussion of the individual case, taking into account all above-mentioned factors. This is also the case for a definite decision whether to clip or to coil.

Because of the potential risk of aneurysm regrowth and of in-stent stenosis with the use of neurovascular stents, careful patient monitoring after endovascular treatment is essential. Patient follow-up is conventionally performed by catheter-based DSA because it provides a high spatial and temporal resolution. However, a disadvantage of this technique is that it only provides 2D information of the vascular anatomy, and the relationship of the vascular anatomy to the stent and coil mass may not be fully appreciated.

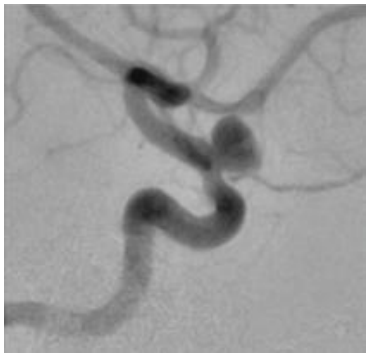

Digital subtraction angiogram of an intracranial aneurysm

The latest generation of angiographic C-arm systems equipped with flat panel technology not only provide conventional 2D fluoroscopy but enable in situ 3D conebeam CT (CBCT) that can be can used for peri-interventional evaluation. Recently, the development and application of high-resolution contrast-enhanced conebeam CT (VasoCT; Philips, Best, the Netherlands) with the use of an angiographic flat-panel C-arm system

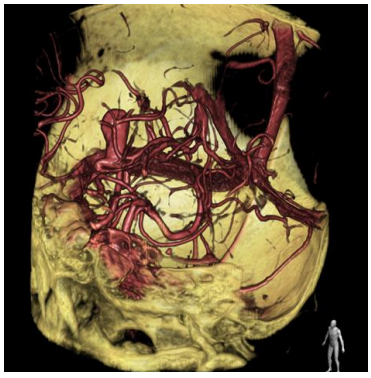

3D CBCT reconstruction of an intracranial aneurysm

has been reported. This technique enables detailed 3D visualization of neurovascular stents and host arteries that allows for a more complete determination of stent-wall apposition and in-stent stenosis. (Bom, 2013.)

In the domain of interventional x-ray imaging, digital subtraction angiography (DSA) and three-dimensional rotational angiography (3DRA) are the gold standard for imaging vascular lesions. Though these provide valuable information regarding the vascular morphology, it is still difficult to extract functional information from DSA. The recent advancements in minimally invasive treatment of vascular lesions, however, could considerably benefit from the availability of quantitative functional measurements during the course of the interventional procedure. For example, the flow pattern inside aneurysms is considered to be one of the parameters that can be used to predict rupture and clotting. Also in stenosis grading, arterio-venous malformations, and post-interventional hyperperfusion flow measurements can be valuable. (Bonnefous, 2012).

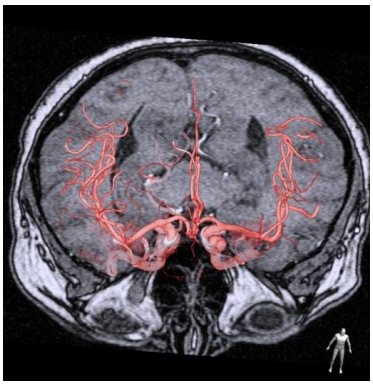

Fused 3DRA and MR

4.3.4 BENEFIT update

Blood flow in aneurysm

Philips has introduced a tool for measuring blood flow through high frame rate X-ray angiography, based on following the contrast density in the vessels modulated by the cardiac phase (Bonnefous, 2012). During the acquisition of the DSA data, iodine contrast agent is injected intra-arterially at a very modest pace (1.5 ml/s). When injecting contrast into an artery, blood and contrast medium mix proportionally to their respective flow rates. Therefore, during systole the dilution of the contrast medium entering the artery is higher than during diastole. The physiological pulsatility of the blood flow therefore adds a periodic modulation on top of a regular dilution of contrast. The low frequent regular dilution is subtracted from the X-ray signal, in order to process only the periodic modulation.

The normalized mean aneurysm flow amplitude ratio (MAFA-ratio) has been introduced as a parameter that can be used to measure the efficacy of the flow diverting stent during the course of the intervention (Pereira V. e., 2013). The MAFA-ratio is defined as the aneurysm flow before and after stenting, normalized by the respective flow in the feeding artery. Preliminary results (Pereira V. e., 2013) (Brina, 2014), as well as validation experiments (Bonnefous, 2012) (Pereira e. a., 2014) (van Nijnatten, 2015) (Cebral, 2017) have shown promising results.

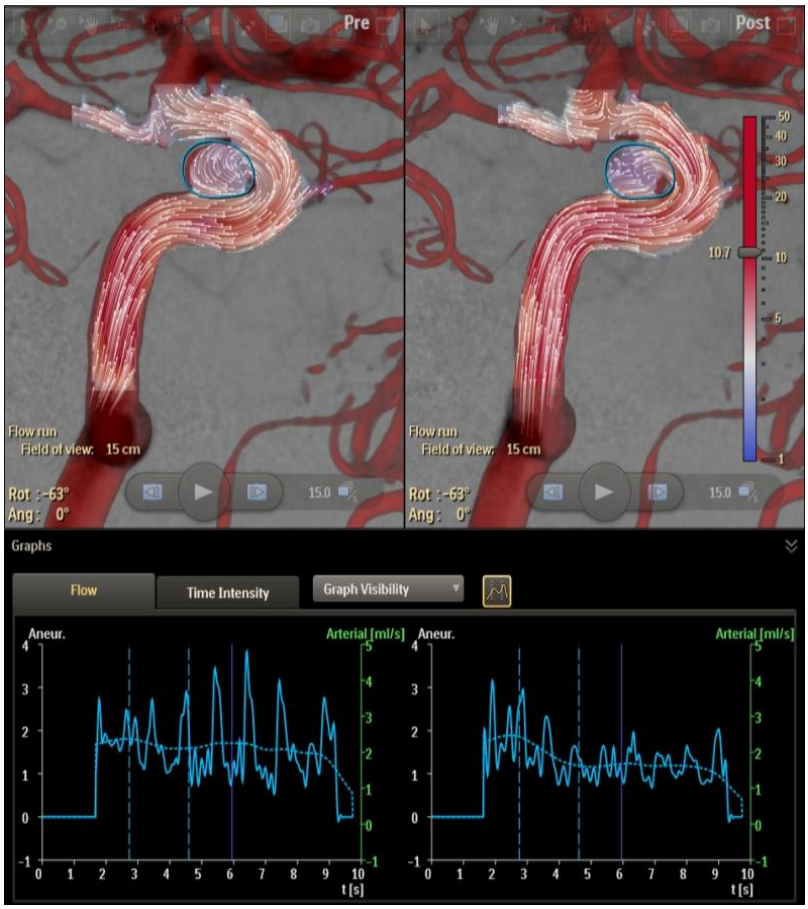

Figure: The Philips AneurysmFlow tool shows the measured flow prior (left) and post flow diverter stent deployment

Cerebral Blood Volume

Cerebral Blood Volume (CBV) is a measure for the amount of blood that enters the brain tissue in a particular location. It can be measured with an angiographic C-arm by a long iodine injection, with the objective to reach a steady state in the brain parenchyma. During the steady state the amount of iodine contrast entering and leaving the parenchyma is the same, leading to a static iodine filling which is representative for the blood capacity of the particular volume. By acquiring a cone-beam CT acquisition during the steady state as well as one before the injection of contrast and by subtracting them, the CBV can be studied. Crucial for the CBV acquisition is reaching the steady state, while minimization of the harmful contrast load renders this in a delicate process. This has been studied in (Caroff, 2014).

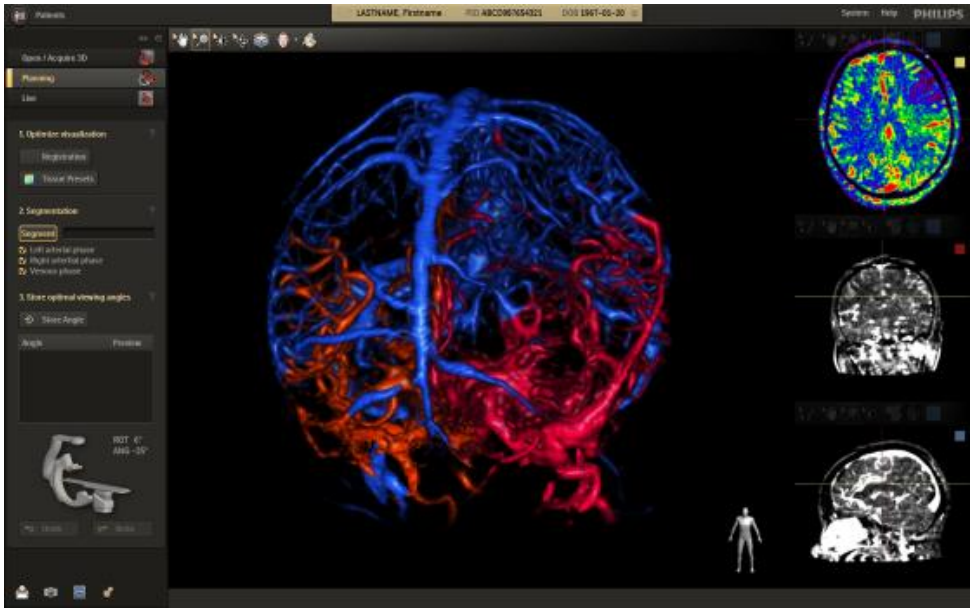

Figure: the Philips CBV prototype software

Navigation support

Stroke decision making, such as determining choice of treatment, and decisions while treating, often lacks sufficient (quantitative) information. Within the Benefit project, technology was developed that may address lack of information and quantitative biomarkers in two ways: (1) by using intra-patient variability such as (a)symmetry of brain hemispheres, and (2) by using population-based variability derived from healthy populationatlas information.

Stroke generally affects only one side of the brain, i.e. either the left or right hemisphere. Symmetry between both hemispheres may provide additional information during interventions, such as the vessel shape, sizelength, diameter and position of arterial branching. To that end, it was investigated to what extent brain vasculature morphology of the proximal MCA was symmetric, and to what extent geometric information about (such as vessel sizesgeometrical properties) from of proximal MCA in the contralateral side hemisphere could be used (Peter, Quantitative Analysis of Geometry and Lateral Symmetry of Proximal Middle Cerebral Artery, 2017). The main results are It can be concluded that there is can be significant a differences in morphology of proximal MCA - especially regarding full length, and that certain geometrical properties of the arterial segment such as diameter, tortuosity, M1-ICA angles (see Figures) are symmetrical in both brain hemispheres and can be used for decision making (e.g. about the size of stent-retriever, navigation of catheter, etc.). Non-rigid registration of the contralateral hemisphere could model ~70% of the ipsilateral M1 segment on average with average distance of 1.5mm between the arterial centerlines. Furthermore, but that the geometry of the proximal segment the location of M1-ACA branching could be determined with average distance of 1.6mm can be used, see details in [Peter et al.]

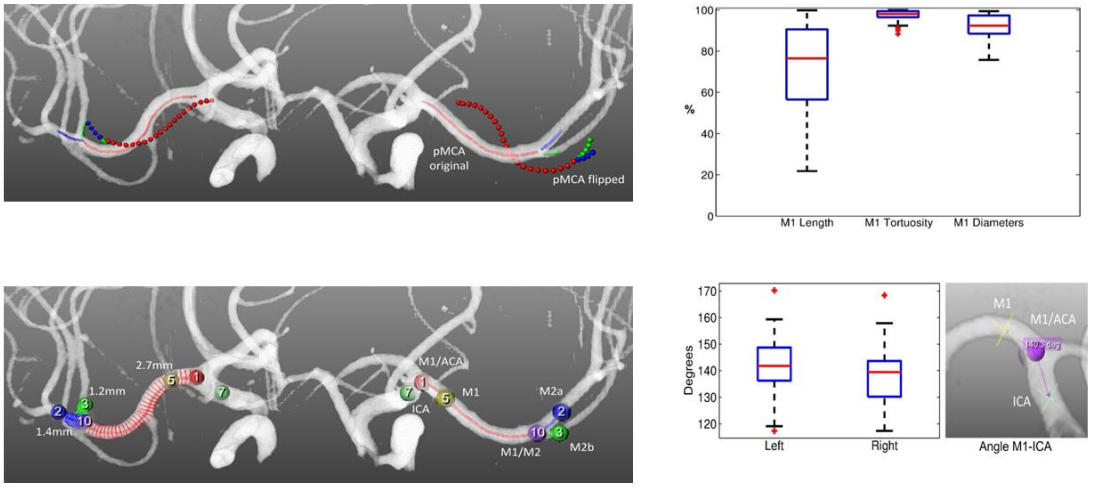

Figure: upper-left: alignment of vessels after flipping of hemispheres. Bottom: landmarks used for assessing symmetry. Right: tortuosity and diameters are fairly symmetric, but there is substantial difference in the length of the M1 segment.

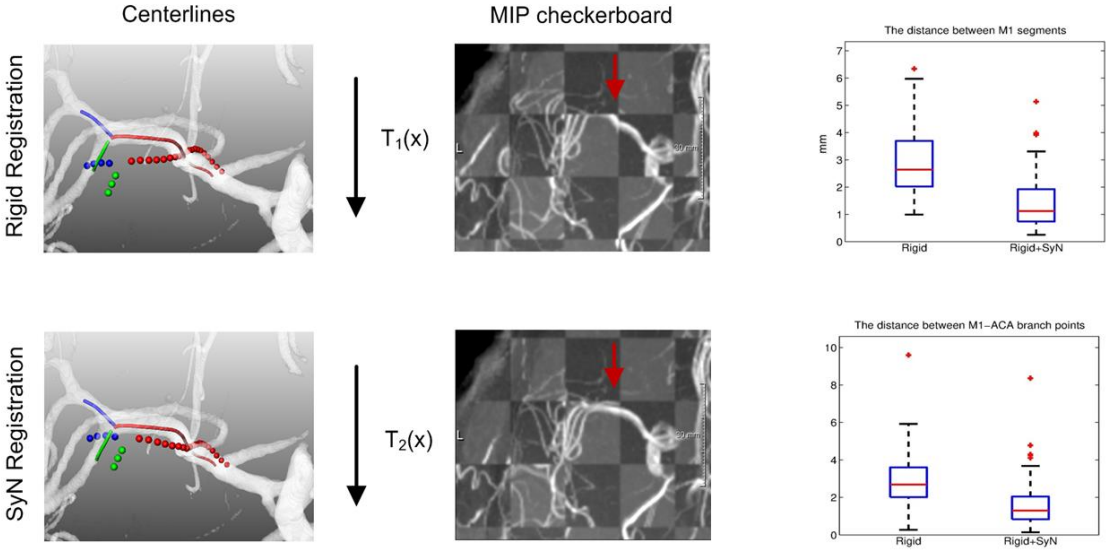

Figure: Difference in rigid (upper row) and non-rigid (bottom row) registration in aligning the proximal MCA.

Additionally, atlas information, such as brain structures, may be used to enrich individual patient images. Within the Benefit project, an atlas of brain structures was build constructed for CTA images, by combining and aligning two different publicly available MR brain image sets to a multimodal MR-CT brain template (Peter, Cortical and Vascular Probability Maps for Analysis of Human Brain in Computed Tomography Images, 2017). The result allows to combine structural and functional brain images with CTA images of a patient acquired , pre-before interventionally and during the intervention (provided that a robust 2D/3D registration is available), see Figure below

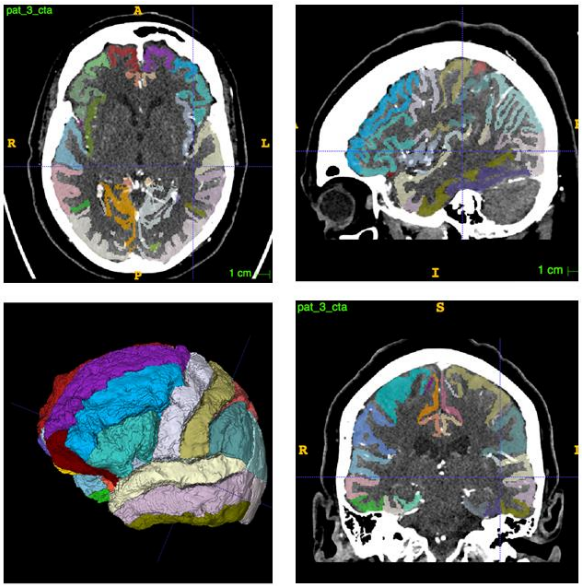

Figure: brain region labeling in patient CT dataset, created by aligning the CT-MR brain structure atlas to a patient CT dataset..

4.4 Liver tumor treatment

Lead authors: UMCU

4.4.1 Introduction

Liver tumors are caused by primary or secondary liver cancer. The most common form of primary liver cancer in adults is hepatocellular carcinoma (HCC). HCC can be caused by a viral infection with Hepatitis B or C, or by cirrhosis, a disease that causes chronic liver damage. Patients with HCCs often do not show symptoms other than caused by the underlying liver disease, and thus these tumors are detected in a late stage, which gives poor survival rates for patients diagnosed with HCCs (5-year survival of 12%, and median survival ranging from 6 – 20 months). Early detection and adequate treatment options thus are required.
Secondary liver cancer implies liver tumors are metastatic, most commonly from primary colorectal cancer, but also from lung or breast cancer.

The 2012 GLOBOCAN global analysis estimated a total incidence of 782.000 of primary liver cancer and a mortality of 746.000 worldwide, with 82% of primary liver cancer cases occurring in developing countries. Colorectal cancer showed a worldwide incidence of 1.360.000 and a mortality of 694.000 [globocan.iarc.fr]. Approximately 50% of colon cancer patients will be diagnosed with hepatic metastases [www.cancer.gov].

4.4.2 Clinical State of the Art

Based upon an analysis of a patient's medical history and initial physical exams, a doctor can suspect the presence of liver tumors. Imaging is used as a first method for diagnosis. Various imaging techniques are available:

- Ultrasound (US),

- Fluoroscopy,
- Computed tomography (CT),
- Magnetic resonance imaging (MRI).

In addition to such exams a full bloodwork analysis is performed. A biopsy may be performed, in which a small portion of suspected liver tissue is removed for accurate pathological examination. A laparoscopy procedure is also sometimes performed as a follow-up to imaging, which involves visual inspection of the liver via a small camera inserted through a minor incision in the abdomen.

The outcomes of the various exams and procedures lead to a diagnosis and staging of the disease. Based on the staging, patient-specific factors, and available procedures in the hospital a treatment plan is composed.
First option is resection of the tumor in the liver (Perini, 2015), or liver transplantation. These are invasive surgical procedures, where the tumor is completely removed by surgery. Not all patients are eligible for these types of surgery, as their health may already be comprised by the underlying liver disease. Varying mortality rates are reported for surgical resection, careful patient selection is thus relevant. Also, survival rates are depending on the stage of the disease, with better survival rates for early stage and single lesions.

Several minimally invasive alternatives for open surgery exist (Li, 2014). Minimally invasive treatments promise benefits over traditional surgery, such as less tissue damage, reduced pain, less scarring, lower risk of complications, shorter or no hospital stays and faster recovery.
Among the minimally invasive alternatives are needle-based approaches, where a needle is brought in through the skin (percutaneously), such that the needle tip is in the tumor. These approaches are often image-guided, using ultrasound or CT to visualize the target anatomy. Examples of these approaches are radiofrequency ablation (RFA), microwave ablation (MWA), cryoablation, and percutaneous ethanol injection (PEI). In the first two approaches, radiofrequency is used to locally heat the tumor, whereas in cryoablation, cooling is used to destroy the tumor, and in PEI, ethanol is injected to kill the tumor. The latter intervention may need multiple sessions. A recently novel approach is irreversible electroporation (IRE), where high voltages are used to damage the tumor cells. All these needle-based approaches are generally associated with low complications rates, but are also considered less effective than surgical resection, and thus are the option of choice if the patient is not able to undergo the surgical procedure.

Transarterial approaches are another class of minimally invasive interventions. In these interventions, instruments are navigated to the tumor via the arterial system. Often, an incision in the groin is made to access the femoral artery, and then via the aorta and the hepatic artery, catheters are brought to the tumor for local treatment. There are several versions of these approaches, such as transarterial embolization (TAE), transarterial chemo-embolizations (TACE) and transarterial radio-embolization. In all cases, embolization is meant to stop the blood supply to the tumor. In case of chemo-embolization, chemotherapy is applied together with the embolization, and in case of radio-embolization, radiotherapy (radioactive isotopes) is combined with embolization (see for example Figure 3). These approaches are generally used for patients for whom resection and the ablation approaches (too many, too diffuse, too large tumors) are not applicable. Transarterial approaches are performed under X-ray and fluoroscopy image guidance. In case of radioembolization additional nuclear

imaging is required to ensure no leakage or shunting of embolizing particles to other critical organs exist.

Stereotactic radiotherapy is an alternative approach. However, the liver is a very radiosensitive organ, which is a major drawback of this approach. Additionally, localization of the tumor during treatment is a challenge.

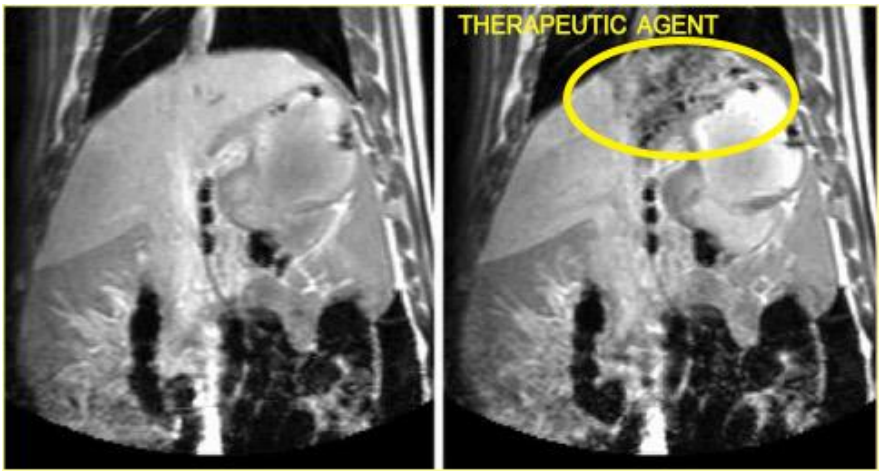

Figure 3 Local drug delivery in the liver. Left: before treatment. Right: after treatment, the therapeutic agent is visible in the top right part of the liver.

Another relatively novel approach is high intensity focussed ultrasound (HIFU). In this approach, high intensity ultrasound waves are focussed at the tumor location, and in that way the tumor is heated and destroyed. HIFU can be performed under MR or US image guidance. Challenges in these approaches are shadowing caused by the ribs (the beam should be send between the ribs), and tumor motion caused by breathing.
Additionally, combinations of aforementioned approaches have been proposed, e.g. using a minimally invasive approach before surgery, or combining stereotactic radiotherapy with other minimally invasive approaches.

4.4.3 State of the art on risk stratification, intervention selection and success evaluation

There are different staging systems for liver cancer in use:

- The TNM system as defined by the American Joint Committee on Cancer
- The Barcelona Clinic Liver Cancer (BCLC) system
- The Cancer of the Liver Italian Program (CLIP) system
- The Okuda system
- The Hong Kong Liver Cancer Staging System.

No comparative analysis/research has been performed with respect to these systems. Currently all four systems are in use in certain parts of the system, with some being more used than others. An example is given in Figure 4.

Risk stratification differs per treatment. Fong's method includes five criteria for hepatic resection for metastatic colorectal cancer based on 1001 consecutive patients: two imaging factors (number and size of metastases) and three oncological parameters

(disease-free interval, carcinoembryonic antigen level and node-positive primary tumor) (Fong, 1999). Stang et al. determined four relevant criteria for RFA of colorectal liver metastases based on a study of 88 consecutive patients: response to systemic therapy, number and size of metastases and carcinoembryonic antigen level (Stang, 2014).

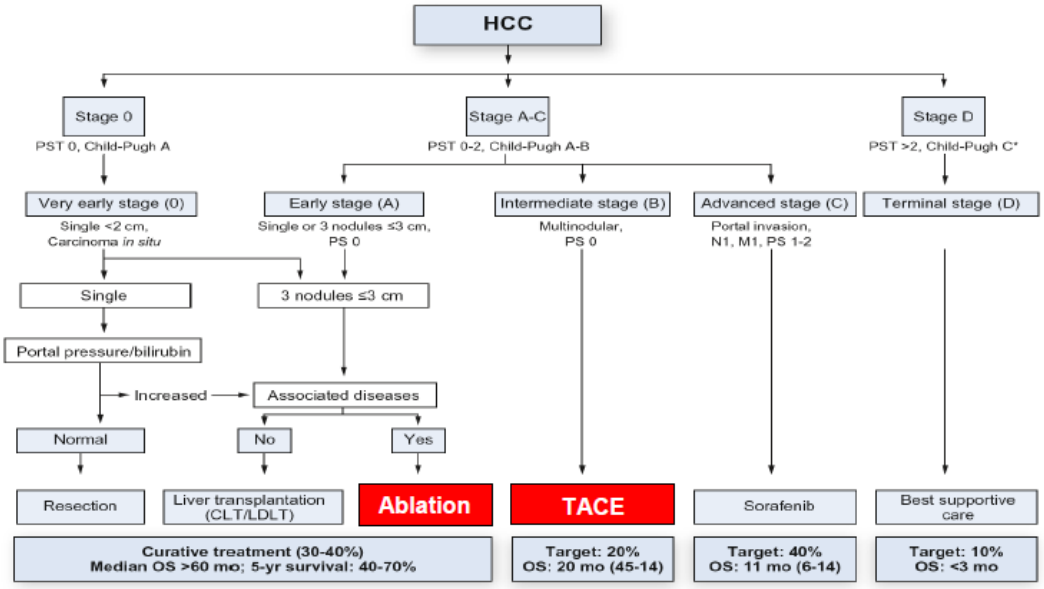

Figure 4 BCLC staging system for liver cancer therapy

In general, there is consensus that surgical resection is associated with the best prognosis for early stage disease, whereas the minimally invasive approaches are used for advanced stages or patients in a bad condition. Resection is however not always safely possible, for example due to a tumor's location close to the main arteries, veins and bile duct and/or comorbidities. Systematic therapy of colorectal liver metastases such as chemotherapy can be used palliatively, but long term overall survival is uncommon. Ablation techniques were initially developed for palliative treatment of unresectable liver tumors. Its success is now leading to an increased number of physicians suggesting the use of RFA in the treatment of both primary and metastatic liver tumors. This extended application of ablation techniques has been increasing in the past years, but prospective studies are required to compare its effectiveness to the gold standard (Higgins, 2006).

The Child-Pugh score is used to assess liver function after (partial) hepatectomy, in combination with various laboratory data and imaging techniques. For RFA and other ablation therapies, initial evaluation is based on imaging and can be performed 24 hours after treatment to confirm the ablation zone and identify any residual tumor tissue. Follow-up imaging is performed weeks to months later.

4.4.4 BENEFIT updates

Philips EmboGuide innovations

Philips is improving upon its EmboGuide and XperCT Dual solution for minimally invasive transarterial chemoembolizations (TACE).

First, Philips is reducing the user-input and time required to plan embolizations during the intervention. Second, Philips is enabling the physician to make more informed decisions about where in the liver to perform selective treatment delivery.

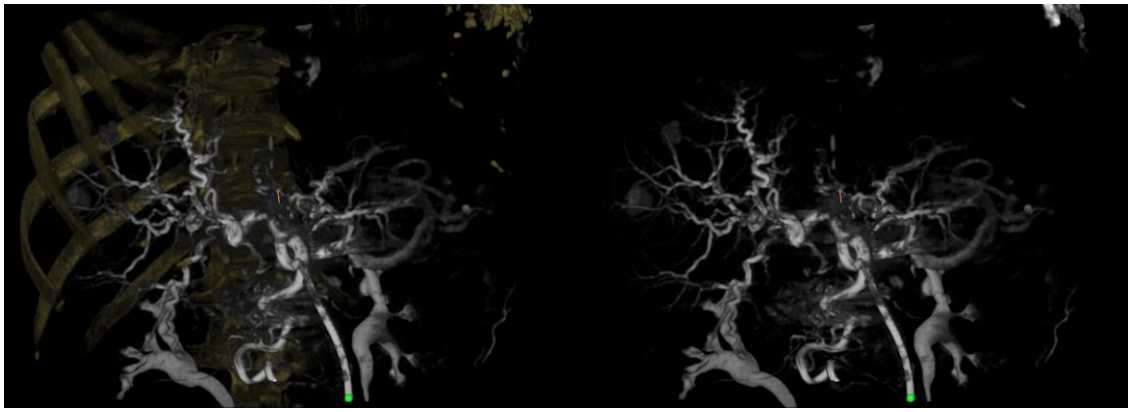

Figure 5 Automatic bone masking improves visibility of liver vasculature with bones

To reduce the amount of user-input, Philips is developing algorithms to automate:
- bone masking, automatically hiding the rib cage and spine in volume presentations of the abdomen, to offer a clear view on the tumors and vasculature
- catheter tip detection, automatically placing a marker on the catheter
- registration of the XperCT Dual arterial-phase and parenchymal-phase scans, to line-up the vasculature from the arterial-phase and tumors from the parenchymal-phase scans even when the patient (diaphragm and liver) moved between the two scans.

These algorithms also present their results quicker than the user would be able manually create these, thereby also reducing the time required to plan the embolization.

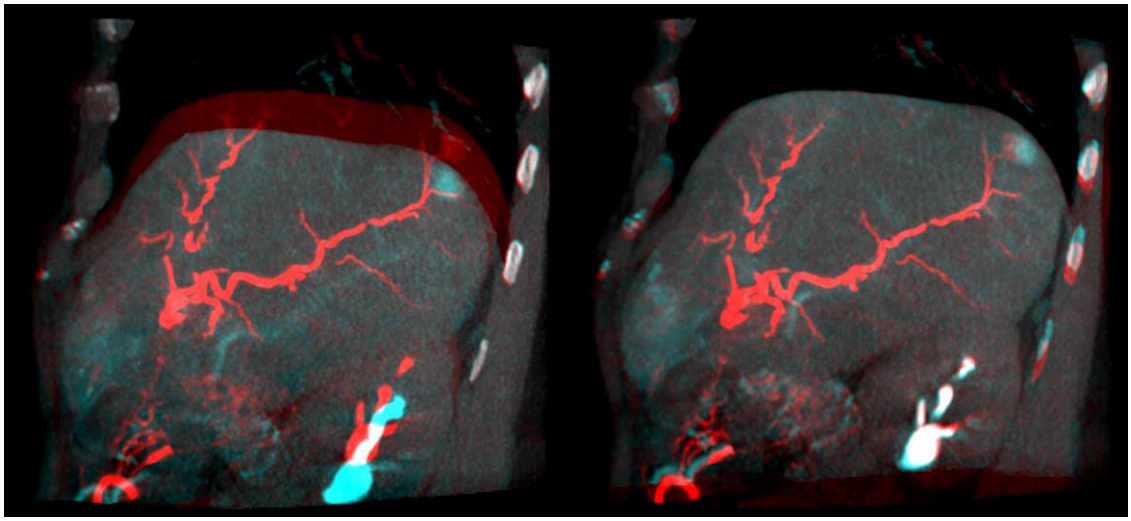

Figure 6 Automatic elastic registration of dual phase scans. On the left, the two scans are overlaid without registration, with ribs lining up but the liver not lining up due to a different position of the patient's diaphragm in the two breath-hold scans. On the right, the liver has been lined up using elastic registration tuned to the liver.

To enable the physician to optimize treatment delivery locations in TACE procedures, Philips is developing 'Virtual Perfusion'. 'Virtual Perfusion' visualizes the effect of embolization from a given location for the liver vasculature and corresponding tissue. This visualization may help the physician to better balance the need to cover the tumor's margin, the need to preserve healthy liver tissue and the ability to reach the planned treatment with a catheter. The visualization can be computed sufficiently fast for the physician to interactively explore treatment delivery.

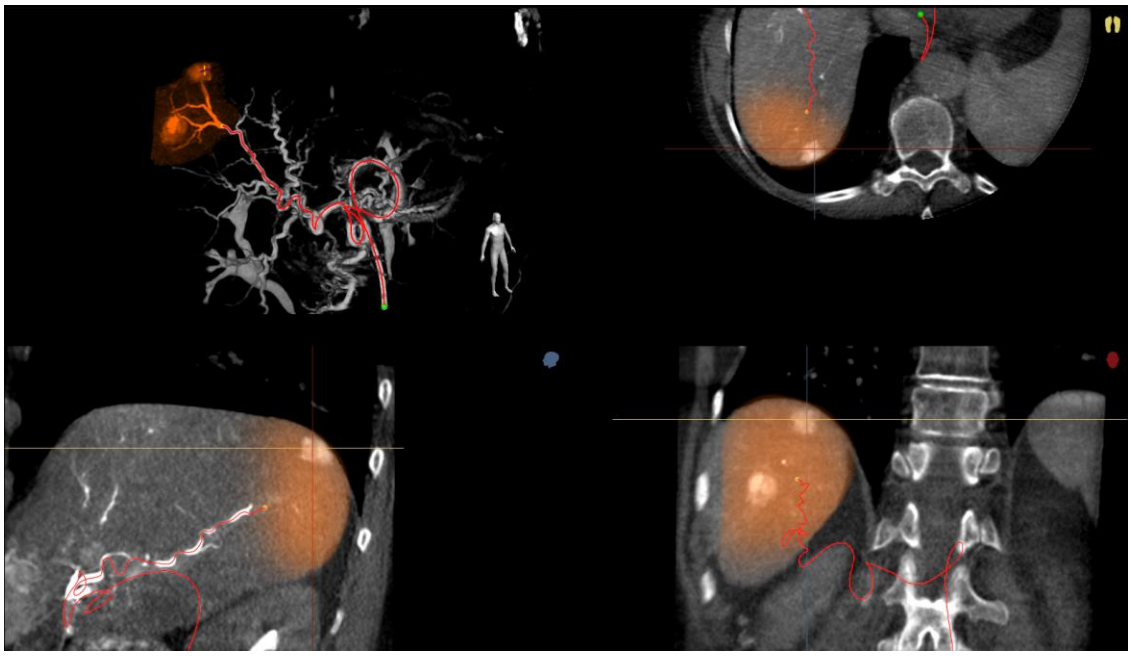

Figure 7 Virtual Perfusion visualized as an orange blush in the 3D volume, and in the axia slices.

Clinical validation of the automated planning steps and of the Virtual Perfusion is currently in progress.

<u>EMC: Alignment of pre- and post-operative images</u>

Conventionally, in percutaneous liver ablation procedures, alignment of pre-operative CT images with interventional CT images (pre-intervention, blanco) to localize a tumor, or alignment of interventional CT images (post-intervention, contrast-enhanced) with post-operative CT images to assess overlap of ablation are performed mentally, i.e. the physician inspects the images, and does the mapping "in his head". Some commercially available systems may offer an automated rigid registration approach. Both the mental mapping and rigid registration approaches work best in cases where there is very little deformation. During interventions, however, patients are generally sedated and respiratory state can not be controlled, which can lead to different respiratory states in between the CT images, which in turm may cause a non-rigid deformation of the liver. Additionally, during interventions, patients are sometimes put

on their side, or in prone position, to give access to the site where the needle needs to be introduced.
The Benefit project has contributed to the development of a non-rigid registration approach (Luu, 2016). In this approach, deformation of the liver can be taken into account, while simultaneously preventing large deformations which would be physically unrealistic.
Additionally, the project contributed to a novel way of evaluating registration accuracy. Often, registration accuracy is measured with Dice (overlap) measures, or mean surface distances. It is well known that Dice is not a good metric, and mean surface distances do not represent the target registration error. Additionally, both metrics quantify errors at the liver border, whereas a lesion may be internal. Using landmarks, as is being done in e.g. lung images, is difficult when aligning liver images without contrast agent, as there are hardly any 3D landmarks available. Therefore, a novel approach has been developed, that uses contrast-enhanced images and generates simulated non-contrast-enhanced images. In this way, the clinical scenario is simulated, and a ground truth is available, as lesion centers can be annotated in both contrast-enhanced diagnostic and interventional images. This method was applied to assess the registration performance: the median target registration error for all non-rigid registrations that were successful (33 out of 35 patients) was 4 mm, vs. a median error for rigid registration error of 9 mm and and for mental mapping of 11 mm.

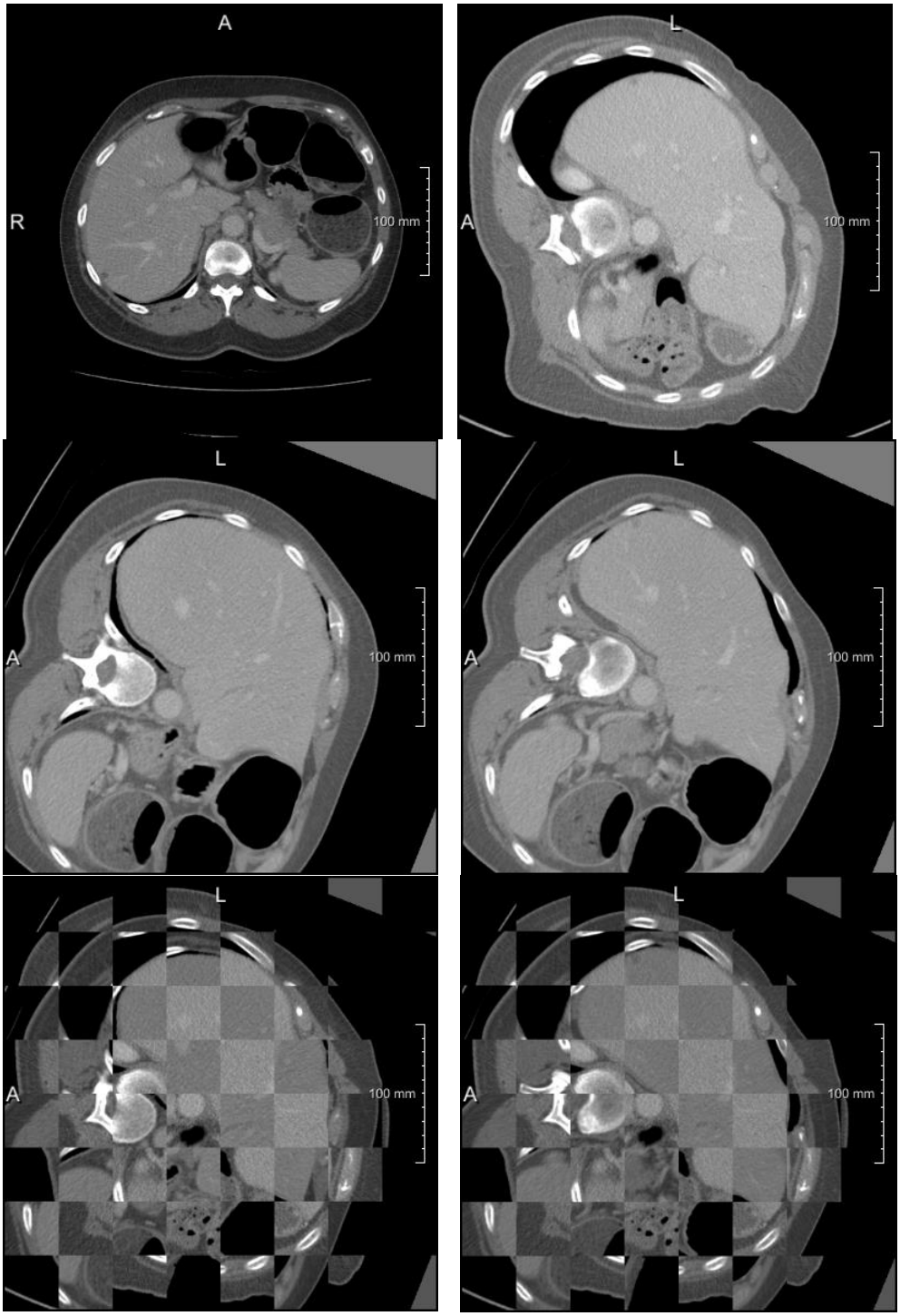

Figure: registration results. Top row: diagnostic image (left) and interventional image (right); middle row: rigid registration (left) and non-irigd registration result of diagnostic image to interventional image; bottom row: checkerboard view of registration results. In the checkerboard views, the original interventional image is combined with the registered diagnostic image. Note that registration only aligns the liver, other organs may be (grossly) unaligned. Bottom left checkboard image shows that the liver border is less well aligned then the bottom right image. Also, the lesion (dark spot at the top of the liver is nicely reproduced in the non-rigid registration: see top right and middle right image.

Needle positioning system

DEMCON has evaluated a novel needle positioning system. The current workflow for image-guided percutaneous techniques is based on a freehand approach. The physician estimates the position of the lesion and the required needle insertion depth and orientation to reach the predefined target. Often, adjustments of insertion angle are needed to minimize the error of the needle tip with respect to the planned target, which leads to an iterative process of estimating, manually (re)positioning the needle and CT scanning to verify the adequacy of the needle tip position. (Arnolli, 2015) Erroneous angle estimations and needle insertions unnecessarily increase tissue damage, patient exposure to X-rays due to repetitive CT scanning, and thus procedural time and costs. (Arnolli, 2015) (Kettenbach, 2015)

During the guided approach, the system is placed onto a rail that is mounted to the CT-table. The process of patient preparation, path planning and entry point retrieval is the same as for the freehand approach. Subsequently, the physician manually positions the operating platform such that the remote center of rotation of the needle guide coincides with the retrieved entry point. Pressing one of the push-buttons automatically initiates the locking system. A new CT-scan of the anatomical region of interest together with the needle positioning system is made. Using these scans, the target and planned path are displayed for review and the position and orientation of the system with respect to the target are determined. The required insertion depth and angles are calculated and after the physician's approval, the needle guide automatically aligns in the according orientation. The physician manually inserts the needle at the calculated depth and a control CT-scan is made to verify the location of the needle tip. Clinical validation is currently in progress.

Motion corrected comparison of liver lesions over time and classification of lesion type

UMCU has concentrated on motion correction of Dynamic Contrast-Enhanced (DCE) MRI time series of liver lesions. Analysis of such images is severely hampered by patient motion from various causes. A correction technique developed by Erasmus MC has been adapted to achieve optimal performance for the particular application of liver DCE-MRI. The resulting method was extensively evaluated against current clinical practice (no motion correction), both by quantitative alignment measures and by clinical experts for added clinical value. Motion correction substantially improved clinical usage of the data: overlap measures of liver lesions over time increased by motion correction (see **Figure 8**, left) and radiologists rated the quality of the corrected series consistently higher (see **Figure 8**, right). Motion correction of the data allows radiologists to employ so-called subtraction images (difference images between contrast-rich and initial, non-contrast images). These show contrast-uptake properties of tissue, which is valuable information for distinguishing lesion type.

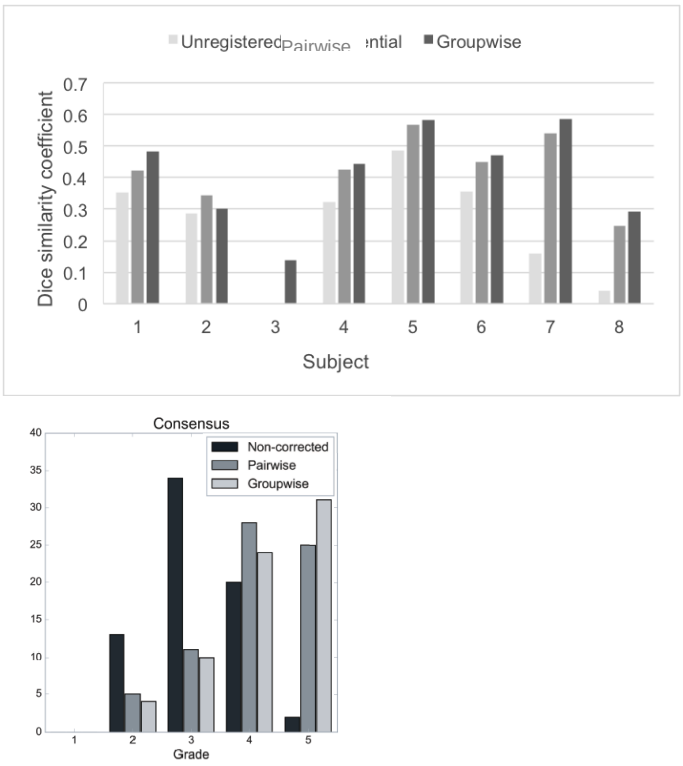

Figure 8 Left: Dice overlap measures of liver lesion delineations for non-corrected, pairwise registered and groupwise registered images. Right: Consensus quality scores of DCE-MRI time series (1-5) by two expert radiologists.

Using the motion correction developed, automatic analysis of DCE-MRI and automatic classification of liver lesion type becomes feasible. A system has been trained on classification of the following lesion types: adenoma, cysts, hemangioma, hepatocellular carcinoma and metastases. It is based on motion-corrected DCE-MRI and T2-weighted MR images. Using feature selection to identify the 15 most distinctive characteristics of the data (see **Figure 9** for examples), an accuracy of 85% for benign versus malignant distinction was achieved on a first evaluation set of 43 patients. Without motion correction, the accuracy was only 64%.

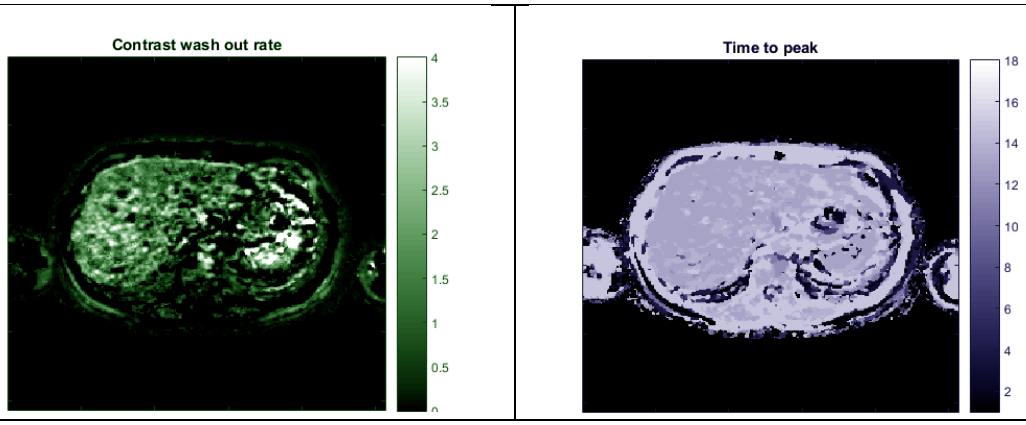

Figure 9 Two features of contrast passage in DCE-MRI images.

4.5 Brain tumors

Lead authors: Elekta

4.5.1 Introduction

Primary brain tumors occur in around 250,000 people a year globally, making up less than 2% of cancers (World Health Organization, 2014). Although primary brain tumors can be either cancerous or noncancerous, both types take up space in the brain and may cause serious symptoms (e.g., vision or hearing loss) and complications (e.g., stroke). All cancerous brain tumors are life threatening (malignant) because they have an aggressive and invasive nature. A noncancerous primary brain tumor is life threatening when it compromises vital structures (e.g., the brainstem).

Tests for brain cancer involve a history, physical exam, and usually a CT or MRI scan; sometimes a brain tissue biopsy is done. Treatments typically include surgery, radiotherapy, radiosurgery, or chemotherapy, often in combination. Depending on the brain cancer type and overall health status of the patient, brain cancer frequently has only a fair to poor prognosis; children have a somewhat better prognosis. Side effects of treatments range from mild to severe.

Primary brain cancer can arise from many different types of brain cells, which affects its characteristics. Based on the microscopic cell appearance, the tumor's aggressiveness is graded on a scale from one to four, where four is the most aggressive.

Among adults, the most common types of brain tumors are:

- **Astrocytoma**: The tumor arises from star-shaped glial cells called astrocytes. In adults, an astrocytoma most often arises in the cerebrum. Based on the tumor grade, astrocytomas are further categorized as follows:
    - Grade I or II astrocytoma: also referred to as a low-grade glioma.
    - Grade III astrocytoma: also referred to as a high-grade, or an anaplastic, astrocytoma.
    - Grade IV astrocytoma: also referred to as a glioblastoma or malignant astrocytic glioma.
- **Meningioma**: The tumor arises in the meninges. It can be grade I, II, or III. It is usually benign (grade I) and grows slowly.
- **Oligodendroglioma**: The tumor arises from cells that make the fatty substance that covers and protects nerves. It usually occurs in the cerebrum. It ismost common in middle-aged adults and can be grade II or III.

Among children, the most common types are:

- **Medulloblastoma**: The tumor usually arises in the cerebellum. Sometimes called a primitive neuroectodermal tumor, it is grade IV.
- **Grade I or II astrocytoma**: In children, this low-grade tumor occurs anywhere in the brain. The most common astrocytoma among children is juvenile pilocytic astrocytoma, which is grade I.

- **Ependymoma**: The tumor arises from cells that line the ventricles or the central canal of the spinal cord. It's most commonly found in children and young adults. It can be grade I, II, or III.
- **Brain stem glioma**: The tumor occurs in the lowest part of the brain. It can be a low-grade or high-grade tumor. The most common type is diffuse intrinsic pontine glioma.

4.5.2 Clinical State of the Art

After a brain tumor has been diagnosed, a multidisciplinary team typically assesses the treatment options. Neurosurgeons typically observe the evolution of the tumor before proposing a management plan. This is only true if benign. For malignant they will want to treat asap. Various types of treatment, detailed below, are available depending on tumor type and location and may be combined to give the best chances of survival. Survival rates depend on the type of tumor, age, functional status of the patient, the extent of surgical tumor removal and other factors specific to each case.

Surgery

The primary and most desired course of action described in medical literature is surgical removal (resection) via craniotomy. Minimally invasive techniques are becoming the dominant trend in neurosurgical oncology (Spetzler, 2012). The prime remediating objective of surgery is to remove as many tumor cells as possible, with complete removal being the best outcome and cytoreduction (partial removal that enhances the effectiveness of radiotherapy or chemotherapy) of the tumor otherwise. In some cases access to the tumor is impossible and impedes or prohibits surgery.

Several current research studies aim to improve the surgical removal of brain tumors by fluorescent labeling of tumor cells (Moiyadi, 2014). Postoperative radiotherapyand chemotherapy are integral parts of the therapeutic standard for malignant tumors. Radiotherapy may also be administered in cases of "low-grade" gliomas, when a significant tumor burden reduction could not be achieved surgically. Single session radiosurgery has an increasing role in the management of such tumors, particularly in the recurrent setting.

Radiotherapy

The goal of radiation therapy is to kill tumor cells while leaving normal brain tissue unharmed. In standard external beam radiation therapy, multiple treatments of standard-dose "fractions" of radiation are applied to the brain. This additional treatment provides some patients with improved outcomes and longer survival rates.

Radiosurgery is a treatment method where a single high dose fraction of radiation, is delivered stereotactically (guided by a three-dimensional coordinate system) to a region of interest while minimizing the radiation dose to the surrounding tissue. Radiosurgery may be an adjunct to other treatments, or it may represent the primary treatment technique for some tumors. It can be performed using machines such as the Leksell Gamma Knife.

Proton therapy is another form of radiation therapy,

Chemotherapy

Patients undergoing chemotherapy are administered drugs designed to kill tumor cells. Although chemotherapy may improve overall survival in patients with the most malignant primary brain tumors, it does so in only about 20 percent of patients. Chemotherapy is often used in young children instead of radiation, as radiation may have negative effects on the developing brain. The decision to prescribe this treatment is based on a patient's overall health, type of tumor, and extent of the cancer. The toxicity and many side effects of the drugs, and the uncertain outcome of chemotherapy in brain tumors puts this treatment further down the line of treatment options with surgery and radiation therapy preferred.

4.5.3 State of the art on risk stratification, intervention selection and success evaluation

For brain tumors, it can be difficult to determine response to therapy and tumor progression in an accurate and reproducible manner. Current responsecriteria vary depending on the pathology and have several limitations. Until recently, the most widely used criteria for gliomas were the "Macdonald criteria" (Macdonald, 1990), based on two-dimensional tumor measurements on computed tomography (CT) or magneticresonance imaging (MRI), in conjunction with clinical assessment and corticosteroid dose. However, the Response Assessment in Neuro-Oncology (RANO) Working Group has published new recommendations in high-grade gliomas (Wen, 2010) and diffuse low-grade gliomas and is working on recommendations for other nervous system tumors. The new recommendations are still based on two-dimensional tumor measurements, although the RANO working group acknowledges its limitations and shows a clear interest in volumetric anatomic assessment. Nevertheless, they did not believe that there was sufficient standardization and availability to recommend adoption of volumetric assessment of tumor volume at the time of the report (2010). Moreover, it was noted that emerging data suggested that advanced MRI techniques such as perfusion imaging (dynamic susceptibility MRI), permeability imaging (dynamic contrast-enhanced MRI), diffusion imaging, magnetic resonance spectroscopy, and [^{18}F]-fluorothymidine and amino acid positron emission tomography may predict tumor response or allow the differentiation of nonenhancing tumor from other causes of increased FLAIR signal.

The evaluation of treatment in high-grade gliomas currently relies either on the duration of patient survival or, more commonly in patients with recurrent disease, the radiographic response rate or progression-free survival. Cognitive evaluations and quality-of-life measurements are increasingly recognized as important end points in clinical trials (Bent, 2011), which is even more true for patients with low-grade gliomas that often present with seizures only. The slow growth pattern of most low-grade gliomas, and the rare radiological true responses despite a favorable clinical response to treatment, interferes with the use of progression-free survival as the primary endpoint in trials.

In current clinical routine, MRI images are evaluated using qualitative (e.g. presence of hyper-intense tissue in an MRI image) or basic quantitative measures such as the maximum tumor diameter measured on axial image slices. Image processing can replace these basic assessments with accurate and reproducible measurements of the relevant tumor and its substructures. Fully automatic image processing routines

and also semi-automatic methods have an enormous potential for improving and speeding up diagnosis, treatment planning and follow-up of individual patients. The number of clinical studies involving brain tumor quantification based on medical images has increased significantly. About a quarter of these studies rely on fully automatic methods. In semi-automatic brain tumor segmentation, user interaction is often used to initialize the method, to provide the possibility of steering the segmentation process, to inspect the accuracy of the segmentation, and to correct the segmentation result. In fully automatic methods, the computer determines the segmentation of tumor without any human interaction.

Developing automatic brain tumor segmentation techniques is technically challenging. Lesions are defined through intensity changes that are relative to the surrounding normal tissue. Partial volume effect and bias field artefacts increase the complexity of the task. Furthermore, tumor structures vary considerably across patients in terms of size, extension, appearance and localization. When growing, lesions can displace normal brain tissues while resection cavities appear after treatment. Finally, in different clinics a large variety of MRI acquisition protocol and sequences are used to image the tumor or tumor-induced tissue changes. This lack of standardization makes it more difficult to develop a general image processing algorithm.

Automatic methods for brain tumor segmentation generally start with preprocessing of the individual images by applying noise filtering, inhomogeneity correction to correct for MRI bias field artefacts and image normalization. In case multiple MRI images are acquired from one subject, automatic image registration is used to align the images to each other on voxel level. Next, image-derived features and prior information are used as input for either generative probabilistic models or discriminative approaches resulting in a tumor segmentation. A generative model combines explicit models of the anatomy and appearance of the tumor region to obtain a segmentation. In this way domain-specific prior knowledge can be incorporated in the segmentation process. However, since the location and appearance of a tumor is hard to predict, encoding prior knowledge is difficult and often the tumor is modeled as an outlier. In addition, if the anatomical model relies on registration of accurately aligned images, problems occur in presence of large lesions or resection cavities. A discriminative approach, often based on pattern recognition techniques, directly learns the relationship between image-derived features and segmentation labels based on example segmentations. In order to be robust, a substantial amount of training data is required. Another drawback is that discriminative approaches explicitly depend on the value of image intensities limiting the application only to images acquired with the same protocol as used for the training images. To overcome the above limitations, joint generative-discriminative methods were developed. These techniques use a generative method in a preprocessing step to create a reliable input for a subsequent discriminative model that can be trained to predict the class labels of the voxels.

An overview of state of the art image processing methods is presented in review articles by Gordillo (Gordillo, 2013) and Menze (Menze, 2014). In the second article, the Multimodal Brain Tumor Segmentation (BRATS) benchmark is presented which allows the comparison of different segmentation methods on a standardized set of data. This set consisted of 65 multi-contrast MR scans of low- and high-grade glioma patients which were manually annotated by up to four raters. Analysis of the inter-rater results showed Dice overlap scores of 74-85% illustrating the difficulty of the task. Automatic methods achieved overlap scores close to the inter-rater variability. The

best results were obtained by methods which employed both a generative probabilistic model and a discriminative approach. Future directions are to include the local certainty, accuracy of the segmentation result, and to evaluate the performance of automatic methods in longitudinal setting as change in tumor structures is often of primary relevance.

4.5.4 BENEFIT updates

In BENEFIT, the treatment planning in Elekta's software Leksell GammaPlan has been improved by introducing important brain areas as organs at risk (OAR) during the treatment planning (to reduce the gamma radiation in these areas). Specifically, image segmentation was used to obtain volumes of the brain stem (blue), the optical nerve (orange), hippocampus (green), chiasma (green), as well as lenses and retina (red), see the Figure to the left. Furthermore, diffusion weighted images were used to generate volumes of certain nerve fiber tracts as additional OARs , see the Figure to the right, as damaging nerve fibers can lead to severe consequences for the patient. All these OARs should receive as little radiation as possible

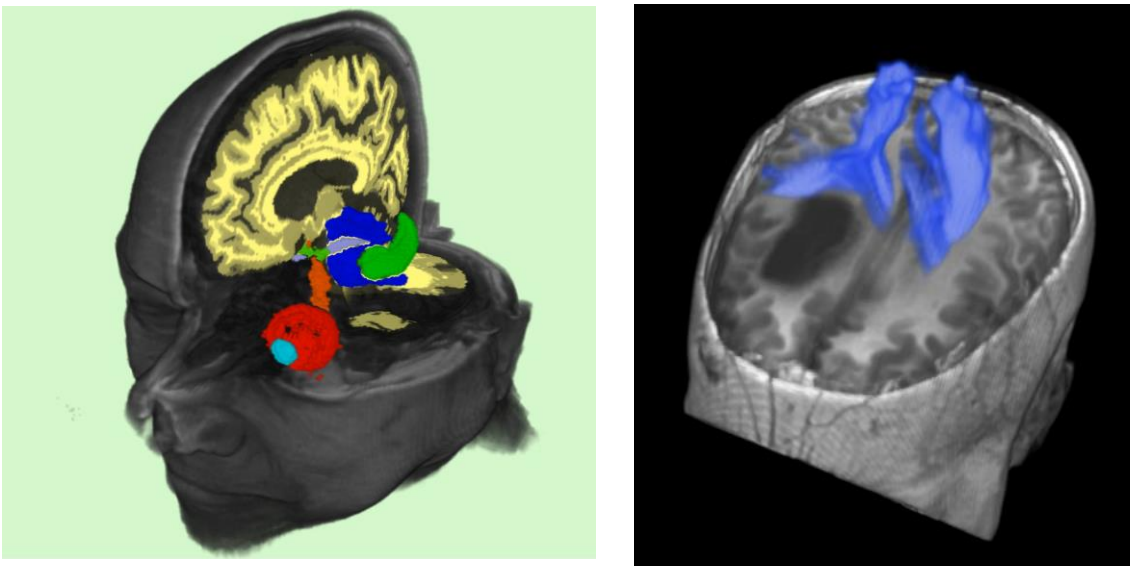

Segmentation of different parts of the brain (left) and nerve fiber tracts (right), to be used as organs at risk during the treatment planning, to reduce the radiation in these areas.

Finally, the automatically segmented brain tumor and the OARs were used to create two treatment plans, one manual (created by an experienced user of GammaPlan) and one automatic (created by solving an optimization problem), see one example in the Figures below. The manual plan took 45 – 60 minutes to generate, while the automatic plan took only 10 – 15 minutes. The mean radiation dose in the organs at risk is similar or lower for the automatic plan. The procedure was repeated for four different subjects and the manual and automatic treatment plans were compared with similar results in all four cases.

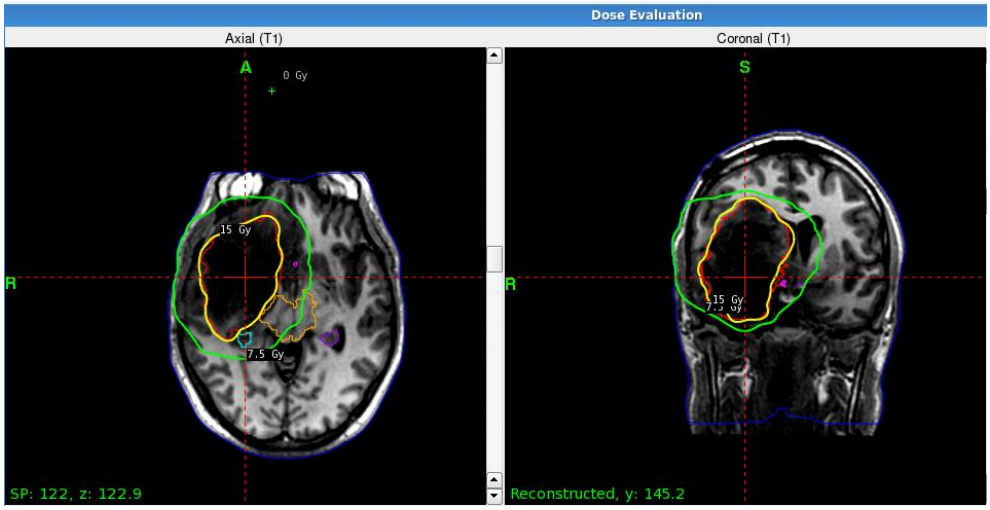

A manually created treatment plan. Target border in red, 15 Gray isoline in yellow, brainstem in light brown, chiasma in purple, hippocampus in cyan.

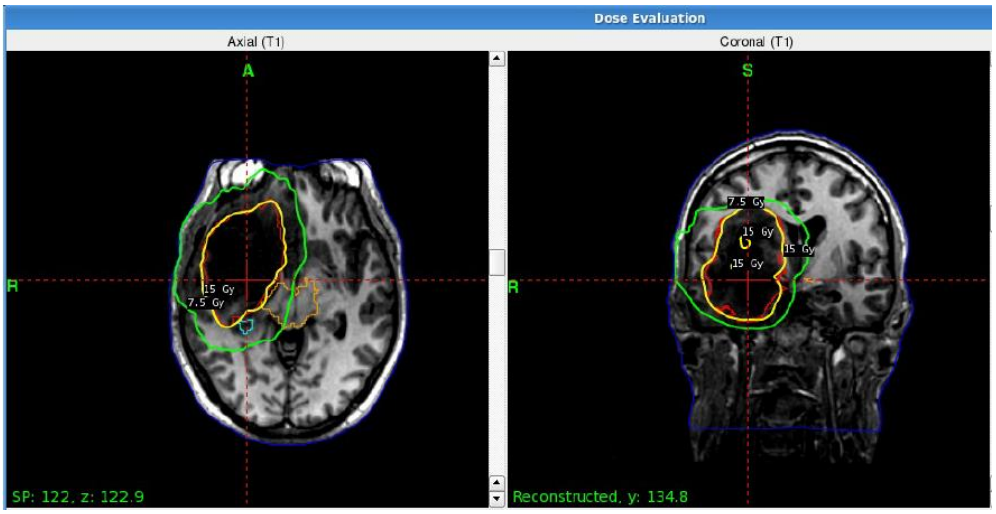

An automatically created treatment plan. Target border in red, 15 Gray isoline in yellow, brainstem in light brown, chiasma in purple, hippocampus in cyan.

5 Bibliography on Clinical Procedures

Aerts, H. (2011, June 1). *D1.1.1 State of the Art in Interventional Therapies.* Retrieved from www.itea3.org: https://itea3.org/project/mediate.html

Arnolli, M. (2015). An overview of systems for CT-and MRI-guided percutaneous needle placement in the thorax and abdomen. *International Journal of Medical Robotics and Computer Assisted Surgery*, 11(4), 458-475.

Bent, M. v. (2011). Response assessment in neuro-oncology (a report of the RANO group): assessment of outcome in trials of diffuse low-grade gliomas. *The lancet oncology*, 12.6: 583-593.

Bom, I. v. (2013.). Reduction of Coil Mass Artifacts in High-Resolution Flat Detector Conebeam CT of Cerebral Stent-Assisted Coiling. *AJNR American Journal of Neuroradiology*, 34: 2163-2170.

Bonnefous, O. (2012). Quantification of arterial flow using digital subtraction angiography. *Medical Physics* , 39(10), 6264-6275.

Brina, O. e. (2014). Intra-Aneurysmal Flow Patterns: Illustrative Comparison among Digital Subtraction Angiography, Optical Flow, and Computational Fluid Dynamics. *AJNR American Journal of Neuroradiology*, 2348-2353.

Caroff, J. e. (2014). Use of time attenuation curves to determine steady-state characteristics before C-arm CT measurement of cerebral blood volume. *Neuroradiology*, 245-249.

Carpentier, A. (1995). The Physio-Ring. An Advanced concept in Mitral Valve Annuloplasty. *Ann Thorac Surg.*, 60:1177-1186.

Cebral, J. e. (2017). Understanding Angiography-Based Aneurysm Flow Fields through Comparison with Computational Fluid Dynamics. *AJNR American Journal of Neuroradiology*, 1180-1186.

Chikwe, J. (2009). State of the Art: Degenerative Mitral Valve Disease. *Heart, Lung and Circulation*, 18:319–329.

Farooq, V. (2013). Anatomical and clinical characteristics to guide decision making between coronary artery bypass surgery and PCI for individual patients: development and validation of SYNTAX score II. *Lancet*, 381:639-650.

Fearon, W. F. (2013). Prognostic Value of the Index of Microcirculatory Resistance measured after primary percutaneous coronary intervention. *Circulation*, 127:2436-2441.

Fong, Y. (1999). Clinical score for predicting recurrence after hepatic resection for metastatic colorectal cancer. *Annals of Surgery*, 230(3):309-318.

Garg, P. (2017). Comparison of fast acquisition strategies in whole-heart four-dimensional flow cardiac MR: Two-center, 1.5 Tesla, phantom and in vivo validation study. *J Magn Resonance Imaging*.

Glower, D. (2014). Percutaneous mitral valve repair for mitral regurgitation in high-risk patients: results of the EVEREST II study. *J Am Coll Cardiol*, 15;64(2):172-181.

Gordillo, N. (2013). State of the art survey on MRI brain tumor segmentation. *Magnetic Resonance Imaging*, Oct;31(8):1426-38.

Higgins, H. (2006). RFA for liver tumors: does it really work. *The Oncologist*, 11(7):801-808.

Ioannidis, J. (2010). What makes a good predictor? *Journal of the American Medical Association*, 303: 1646-1647.

Iung, B. (2003). A prospective survey of patients with valvular heart disease in Europe: The Euro Heart Survey on Valvular Heart Disease. *Eur Heart Journal*, 24(13):1231-1243.

Kamphuis, V. (2017). In-scan and scan-rescan assessment of LV in- and outflow volumes by 4D flow MRI versus 2D planimetry. *J Magn Reson Imaging*, Jun 22.

Kettenbach, J. (2015). Robotic systems for percutaneous needle-guided interventions. *Minimally Invasive Therapy & Allied Technologies*, 24(1), 45-53.

Li, D. (2014). Minimally invasive local therapies for liver cancer. *Cancer Biol Med*, 11(4):217-236.

Liu, S. (2016). Analysis and compensation for the effect of the catheter position on image intensities in intravascular optical coherence tomography. *Journal of Biomedical optics*, (21)12.

Loewenstein, J. (2012). The Natural History and Treatment Options for Unruptured Intracranial Aneurysms. *International Journal of Vascular Medicine*, AID 898052.

Luu, H. (2016). Non-rigid registration of live CT images for CT-guided ablation of liver tumors. *PLOS ONE*, 11 no. 9.

Macdonald, D. (1990). Response criteria for phase II studies of supratentorial malignant glioma. *J Clin Oncol*, 8:1277-1280.

Makkar, R. (2014). Stratification of outcomes after transcatheter aortic valve replacement according to surgical inoperability for technical versus clinical reasons. *J Am Coll Cardiol* , 63:901–911.

Menze, B. (2014). The Multimodal Brain Tumor Image Segmentation Benchmark (BRATS). *IEEE Transactions on Medical Imaging*, p.33.

Moiyadi. (2014). Fluorescence-guided surgery of malignant gliomas based on 5-aminolevulinic acid: paradigm shifts but not a panacae. *Nature Reviews Cancer*, 14.2: 146.

Nishimura, R. (2014). AHA/ACC Guideline for the Management of Patients With Valvular Heart Disease. A Report of the American College of Cardiology/American Heart Association. Task Force on Practice Guidelines. *Journal American Coll Cardiology*, 63(22):e57-e185.

Osnabrugge, R. (2015). Health Status After Transcatheter Aortic Valve Replacement in Patients at Extreme Surgical Risk: Results From the CoreValve U.S. Trial.; CoreValve U.S. Trial Investigators. *JACC Cardiovasc Interv.* , 8(2):315-323.

Pereira, e. a. (2014). Quantification of Internal Carotid Artery Flow with Digital Subtraction Angiography: Validation of an Optical Flow Approach with Doppler Ultrasound. *American Journal of Neuroradiology*, 156-162.

Pereira, V. e. (2013). A DSA-Based Method Using Contrast-Motion Estimation for the Assessment of the Intra-Aneurysmal Flow Changes Induced by Flow-Diverter Stents. *AJNR American Journal of Neuroradiology*, 808-815.

Perini, M. (2015). From minimal to maximal surgery in the treament of hepatocarcinoma: a review. *World journal of hepatology*, 7(1):93-100.

Peter, R. (2017). Cortical and Vascular Probability Maps for Analysis of Human Brain in Computed Tomography Images. *IEEE 14th Intern Symposium on biomedical imaging*, 1141-45.

Peter, R. (2017). Quantitative Analysis of Geometry and Lateral Symmetry of Proximal Middle Cerebral Artery. *Journal of stroke and cardiovascular diseases*.

Petraco, R. (2014). Real-time use of instantaneous wave–free ratio: Results of the ADVISE inpractice: An international, multicenter evaluation of instantaneous wave–free ratio in clinical practice. *American Heart Journal*, 168 (S): 739-748.

Putera, M. (2015). Translation of acute coronary syndrome therapies: From evidence to routine clinical practice. *American Heart Journal*, 169:266-273.

Rosenkrantz, A. (2015). Clinical utility of quantitative imaging. *Academic Radiology*, 22:33-49.

Shahzad, R. (2018). Automatic Quantification of Pulse Wave Velocity: Application for population-based CMR studies. *to be presented at CMR 2018 conference, Barcelona*.

Spetzler, R. (2012). The quiet revolution: retractorless surgery for complex vascular and skull base lesions. *Journal of Neurosurgery*, 116(2):291-300.

Stang, A. (2014). Selection criteria for radiofrequency ablation of colorectal liver metastases in the era of effective systemic therapy. *BMC Cancer*, 14(1):500.

Steiner, T. (2013). European Stroke Organization Guidelines for the Management of Intracranial Aneurysms and Subarahnoid Haemorrhage. *Cerebrovasc Dis (35)*, 93-112.

van Nijnatten, F. e. (2015). Mean Aneurysm Flow Amplitude Ratio Comparison between DSA and CFD. *MICCAI* (pp. 485-492). Munich: Springer.

Wen, P. (2010). Updated response assessment criteria for high-grade gliomas: response assessment in neuro-oncology working group. *Journal of Clinical Oncology*, 28.11: 1963-1972.

WHO. (2014, May). *The top 10 causes of death.* Retrieved from http://www.who.int/mediacentre/factsheets/fs310/en/.

Windecker, S. (2015). 2014 ESC/EACTS Guidelines on myocardial revascularization. *EuroIntervention*, (10), 1024-1094.

World Health Organization. (2014). *World Cancer Report 2014, Ch 5,6.* ISBN 9283204298.

6 Imaging Procedures

In total 4 imaging techniques are addressed in this document:

- High Quality X-ray Imaging
- Intravascular Ultrasound and Optical Coherence Tomography
- MRI and Cone-beam CT
- Laparoscopic Imaging

This is by no means an exhaustive study of all imaging techniques used in and around intra-interventional imaging. The selection made here is focused on the imaging techniques used in BENEFIT, and especially in the Use Cases defined for the project.

All these techniques are described in a standard way. In the first section, a short introduction is given that provides the background & context of the imaging technique. The second section describes the state of the art of the imaging technique. The last section provides the relation to the clinical usage.

6.1 High Quality X-ray Imaging

Lead author: Philips Healthcare

6.1.1 Introduction

The dynamics of coronary atherosclerosis (progression and regression of coronary atherosclerotic lesions), the healing of lesions, and the development of new lesions, have intrigued cardiologists since the time that this process could be followed by repeated coronary X-ray Angiographic (XA) examinations [Oudkerk], [Bruschke], [Jukema].

Image guidance during the procedure is performed by mono- or biplane fluoroscopy (see Figure 1), which visualizes the guide wires and catheters (some of which have additional markers for improved visibility). The coronary arteries are visualized by injections of contrast agent, which result in a transient visualization of the vessels.

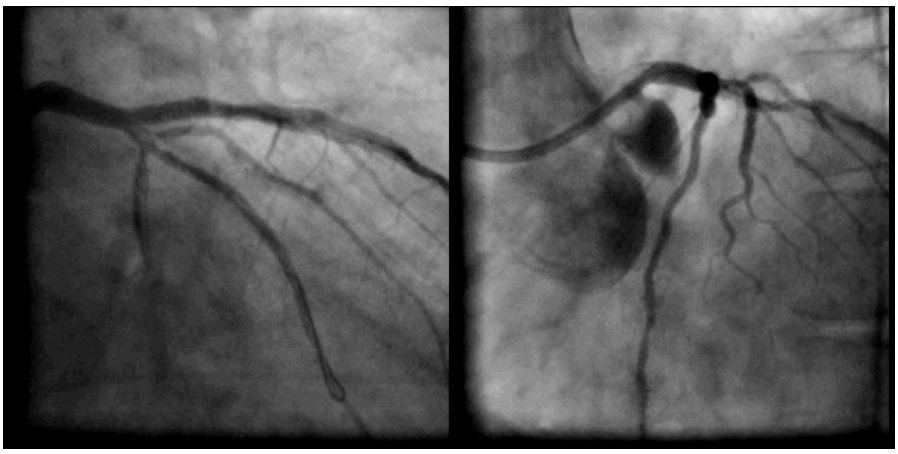

Figure 10: Biplane image of coronary intervention (Image courtesy Erasmus MC)

6.1.2 Technical State of the Art

The technology of XA imaging systems has progressed over the years (starting from conventional vacuum-tube image intensifier) and has resulted in completely digital flat-panel detectors. The advantages of these flat-panel detectors are obvious, the ability to preserve significantly more of the original signal (e.g. due to the large reduction of veiling glare (the scattering process within the image intensifier) and the absolute absence of spatial distortions (e.g. the magnetic field distortion and pincushion distortion, the last one being due to the curvature of the input screen of the image intensifier [van der Zwet], [Holmes], providing better image quality and enabling further image enhancement. In clinical practice, this means an improved visibility of vessels, lesions, and guide-wires, even at reduced X-ray dose levels [Geijer], [Tsapaki]. Typical matrix sizes for the flat panel systems nowadays are 1024x1024 pixels at 12.5 to 30 frames/s, using 8, 10 or 12 bits pixel depth for cardiac acquisitions.

6.1.3 Usage in intervention and treatment evaluation

Using XA imaging is the de facto gold standard for coronary interventions for decades. Both diagnostic and interventional procedures are guided by XA imaging. Treatment and device selection can be done both visually by clinicians as well as supported by quantitative methods like QCA [Reiber], [Lansky]. In interventional cardiology, QCA has been used for on-line vessel sizing for the selection of the interventional devices and the assessment of the efficacy of the individual procedures, for the on-line selection of patients to be included or excluded in clinical trials based on quantitative parameters (e.g. small vessel disease), and for training purposes. Further, it has been applied worldwide in core laboratories and clinical research sites to study the efficacy of these procedures and devices in smaller and larger patient populations [Reiber].

6.1.4 BENEFIT updates

In the examples of the previous section quantification is performed in single images and used for patient selection and treatment support. BENEFIT has added quantification based on the combination of multiple images.
In QFR calculations (section 4.2.4) the vessel lumen diameters from 2 2D projections are combined in an improved 3D lumen profile, which allows for CFD calculations of flow and supports the decision whether to treat a local obstruction yes or no..
In the MAFA calculations (section 4.3.4) the injected contrast medium is detected in successive images and followed in time to deduce parameters for local flow velocity before and after treatment: this seems to be a reliable predictor for the chance for long term treatment success.

6.2 Intravascular Ultrasound and Optical Coherence Tomography

Lead author: LUMC

6.2.1 Introduction

Percutaneous coronary intervention (PCI) is one of the treatment options for patients with chronic stable angina (chest pain due to ischemia of the heart muscle). Whereas PCI is less invasive than other approaches, it is favorable for patients.

However, the preferred treatment depends on various issues, such as patient characteristics and classification of a lesion. The interventions do not cure the underlying cause of the atherosclerotic disease process but they are carried out to alleviate the symptoms and have a survival benefit for the patients.

Coronary X-ray angiography currently is the standard modality for assessing coronary lesions, and a vessel diameter of 50% or less (75% area) is considered a significant lesion. However, the hemodynamic significance of a coronary lesion does not correlate well with stenosis measurements. Therefore other imaging techniques and quantitative measurements are nowadays investigated and employed during the intervention, to decide whether a lesion needs treatment. These modalities, Intravascular Ultrasound (IVUS), Optical Coherence Tomography (OCT) and Fractional Flow Reserve (FFR), provide additional information on the plaque burden and the plaque composition, and can indicate the hemodynamic significance of a coronary lesion.

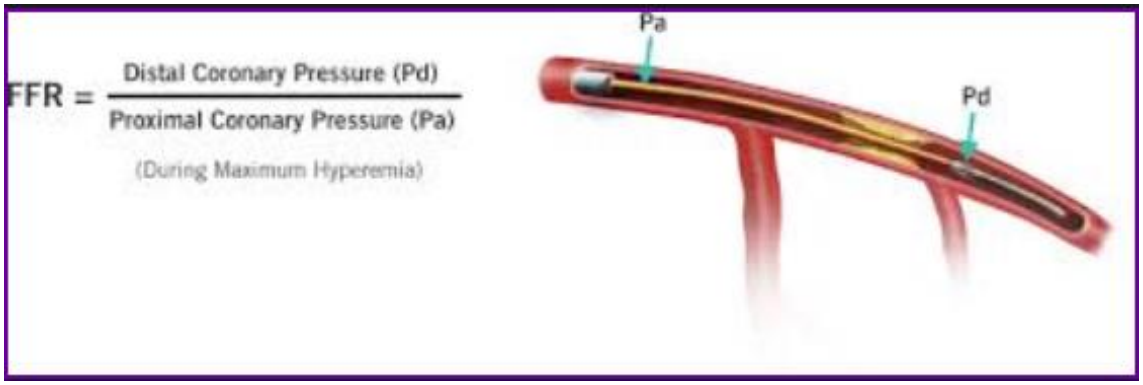

Figure 11: Illustration of the FFR measurement through a pressure wire

6.2.2 Technical State of the Art

Current IVUS systems can image a coronary with 45 Mhz, 30 frames per second, pullback speed of 0.5 mm/sec and a resolution of 100 micron. The quantification of images on-line is limited to single frame measurements by manual contouring. Some systems provide additional information by analyzing the RF signal and show tissue classification as overlay on the IVUS image.

Current OCT systems image the coronary artery with a speed of 180 frames per second and a pullback speed up to 36 mm/sec, Meaning that a segment of 100 mm can per visualized in 3 seconds. The resolution is about 10 micron. Some automatic processing is done on the console by automatic delineation of the lumen. No processing is available for stent detection or tissue classification on the console. For offline analysis, some software is available for lumen detection and stent strut detection. Tissue classification is still in its early stage.

6.2.3 Usage in intervention and treatment evaluation

The purpose of PCI is to restore the vascularization of the heart muscle by widening stenotic lesions in coronary arteries. To this end, a stent is placed in the coronary artery, possibly after prior dilation with a balloon. The procedure is performed minimally invasively, often via the femoral artery. First a guide catheter is introduced,

to provide a safe access of the guide wires and catheters to the coronary arteries. Subsequently, a guide wire is inserted through this catheter, and advanced beyond the lesion. Through this, intravascular imaging (IVUS, OCT, FFR) can be performed.

Intra-arterial imaging with IVUS or OCT is used to assess the vessel wall condition and to characterize the obstructing tissue (plaque). An FFR measurement from a pressure wire is used to determine the hemodynamic significance of a lesion.

Furthermore, the landing zone of the stent can be selected, not only based upon the narrowing of the vessel, but also based upon the condition of the vessel wall proximal and distal. If necessary, it can be decided to place a longer stent to cover vulnerable plaque.

After stenting, it should be checked whether all the struts are positioned against the lumen wall and no struts are blocking an important side branch. If so, additional ballooning will be needed to improve the stent placement.

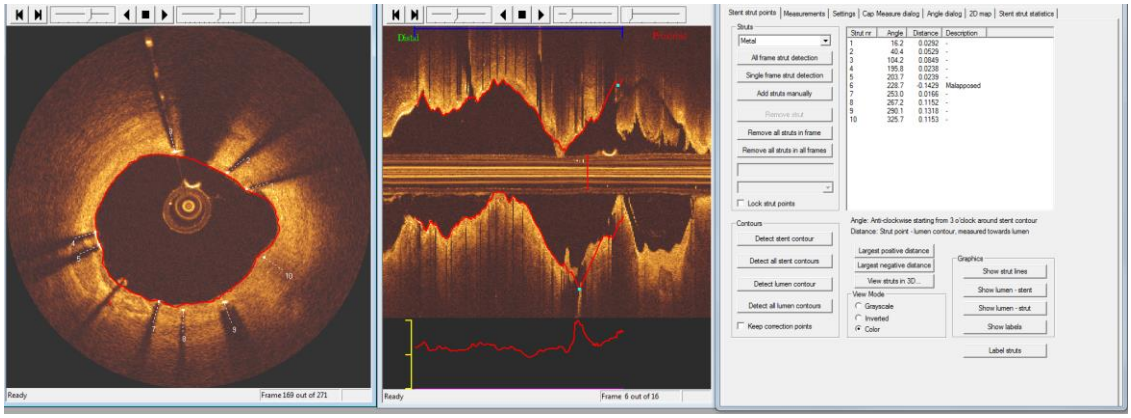

Figure 12: Example of OCT imaging (Image courtesy LUMC)

6.2.4 BENEFIT updates

In BENEFIT progress has been made to check automatically whether the struts are positioned properly against the vessel wall. The border of the vessel lumen and the stent struts are determined according to the following steps:

- The lumen border is detected using the so-called “mincost approach” in both the longitudinal and transversal images. In the images it is looked for dark to bright interfaces (blood-intima interface) and next the candidate points are connected to each other taking into account that the lumen contour should be continuous and have a more or less round shape. The results of the detection are evaluated by comparing them to the automated detected contour with contours from two experts.
- To use the manual corrections as efficient as possible, three methods of correction were implemented; the user can move marker points which guide the longitudinal detection and result in a 3D correction of the lumen contours, the user can insert a correction point in the transversal image and the user can manually draw the contour

- The stent struts are detected by looking at the combination of a bright to dark and a dark to bright interfaces with a certain distance between them. The candidate points are connected using a “mincost approach” to create a box with a minimal width to be a valid strut. From the “black core” box, the endoluminal and abluminal interface is determined and used to create two stent contours. The method is evaluated by comparing the results with manually defined strut boxes and calculating the dice index.

  Stent strut detection

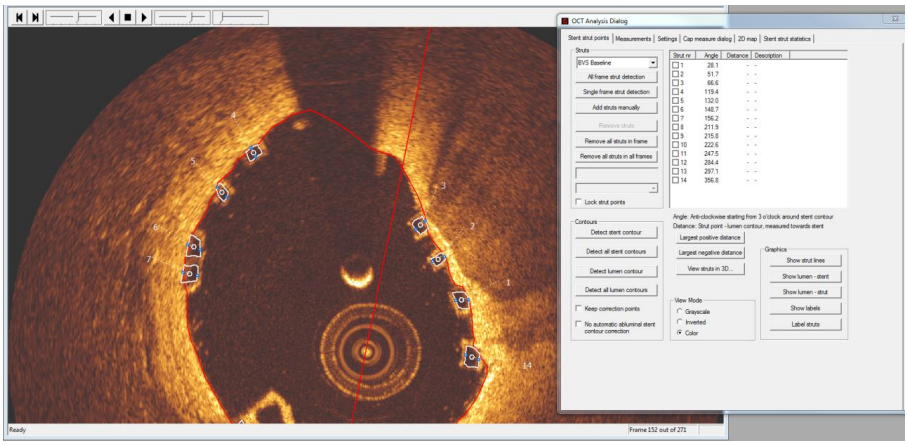

- The struts can be corrected by moving the center of the box, followed by a new detection, or by editing the boxes.
- The position of the strut is determined to calculate the distance between the abluminal interface and the lumen contour. If this distance is larger than 25 micron, the strut is considered to be malapposed. 25 micron is determined by the point spread function of OCT.
- From each strut, the start and end angle is determined with respect to the catheter center. These values are plotted in a so-called “carpet view” to show the distribution of the struts.

Carpet view of stent struts in OCT

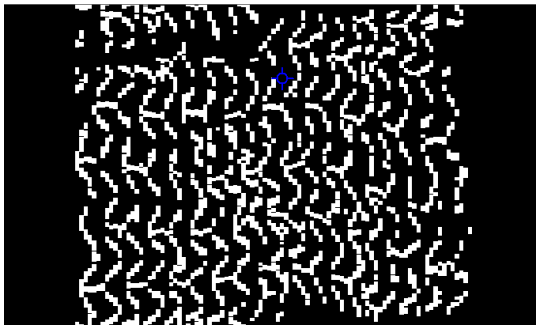

3D view of stent struts

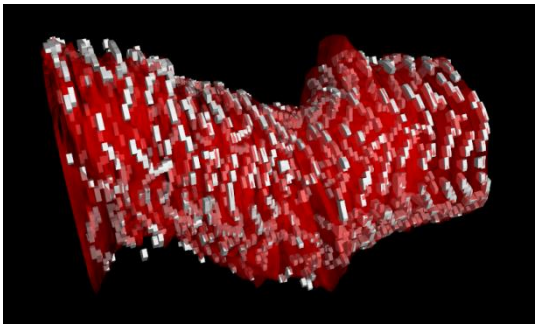

First clinical results have been described in section 4.2.4. In a cohort of 8 patients with almost 8000 struts, the average score of true positives was 89.8%, 8.8% for false positives and 8.3% for false negatives.

6.3 MR Imaging and Cone-beam CT for radiation treatment

Lead authors: Elekta

6.3.1 Introduction

MR Imaging has become the standard imaging modality for soft tissue visualization of organs inside the human body. This enables distinction of different anatomical structures, i.e. in the brain, with a high degree of geometrical accuracy. Cone-beam CT has limited soft-tissue visualization capabilities but instead has a superior visualization of bony structures. To combine these imaging modalities in an intelligent way to enable accurate treatment of the brain with i.e. radiation has been the objective for some time.

6.3.2 Technical State of the Art

For brain surgery using the Leksell GammaKnife the preferred MR imaging uses at least a 1.5T MR scanner. Depending on the anatomical target, different sequences are used. Either T1, T1 contrast-enhanced or T2 are preferred. To optimally visualize glioblastoma as is the target in BENEFIT, the normally used MR sequences are T1, T1 contrast-enhanced, T2, and T2 FLAIR.

When additional resolution of the image set is needed, the option exists to use higher field strengths, like 3T machines.

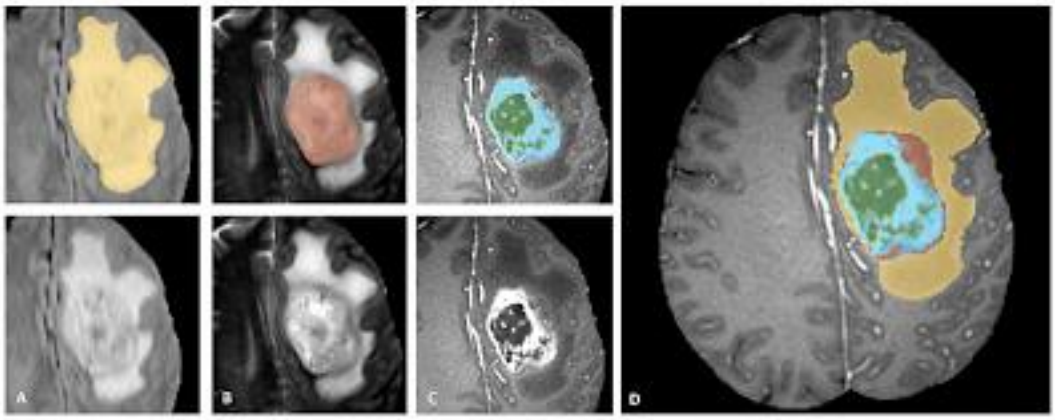

Figure 13: FLAIR imaging (image A), the tumor core in T2 (image B), the enhancing tumor structures in T1c (blue), surrounding the cystic/necrotic components of the core (green) (image C). The segmentations are combined to generate the tumor structures (image D). (Image courtesy http://braintumorsegmentation.org/)

CBCT is a common modality used to determine the position of the patient's head in radiotherapy. CBCT has recently been introduced as part of the Leksell GammaKnife Icon system. Due to the high geometrical precision required in radio surgery it is very important that the CBCT has a very high mechanical precision but also that the registration accuracy between the planning MR and the CBCT is highly accurate. The Icon system has an average mechanical accuracy of 0.2 mm and an average registration uncertainty of 0.3 mm.

6.3.3 Usage in intervention and treatment evaluation

The usage of CBCT during intervention has been standard procedure for about 10 years in traditional Radiation therapy. It has been used to verify the correct positioning of the patient on the treatment table, before initiating the treatment.

The intent of the introduction of CBCT in Radiosurgery using the Leksell GammaKnife has been to verify the correct positioning of the patients' head, independently, before initiating the single-session or multi session treatments. As experience is gained it has become clear that the CBCT functionality greatly facilitates the introduction of fractionation therapy into the Leksell GammaKnife way of treating patients. This is probably (has to be validated) of great importance when treating Glioblastomas.

6.3.4 BENEFIT updates

Diffusion weighted imaging can aid brain tumor treatment planning, by for example providing information about the location of important nerve fiber tracts (which can be damaged during resection or radiation of the tumor), see section 4.5.4. In BENEFIT we applied a tractography algorithm to diffusion weighted images from the patient. Tractography involves setting one or several starting points, and then following the main direction given by a diffusion tensor (a 3 x 3 matrix) in each voxel. Specifically, we used probabilistic tractography, which can handle crossing fibers by repeating the fiber tracking many times, and each time selecting one direction (fiber) from the diffusion tensor. The starting points were generated by registering a white matter atlas to the brain volume of the patient. The generated nerve fiber tracts were finally converted to the DICOM RT struct format, to be read by Elekta's Leksell GammaPlan software.

While MR imaging advances, image analysis tools should work with the existing images as well as images based on improved MR protocols. Also, image analysis tools should be robust to pathology. In this case, Quantib improved its organ at risk software (see section 4.5.4) so it is robust for MR images from different vendors and protocols and added a feature to the software tool so it can handle images with a brain tumor. The tool now has an optional input for a region of interest to exclude during automated segmentation of the organs at risk. In this case, the input is a segmentation of the brain tumor, which can be manually created or automatically. The latter was demonstrated by Linkoping.
In some cases it is necessary to divide a treatment into several fractions taking place over the course of several days. This requires accurate determination of the patient's position before each fraction. With Elekta's Leksell GammaKnife Icon, stereotactic treatments can be delivered without the use of a stereotactic frame fixated to the patient's skull. This improves the possibility to perform fractionated treatments. The skull position is determined with a CBCT prior to each treatment. An automatic co-registration of the CBCT and the CT image used for treatment planning, is done to a precision of 0.3 mm. Then the treatment planning system automatically determines the new shot positions and recomputes the dose distribution and then the dose of the fraction can be accurately delivered.

6.4 Laparoscopic Imaging

Lead author: Barco

6.4.1 Introduction

As illustrated in the figure below, in an operating room multiple unrelated visualization devices are present, mostly cameras linked to displays, mostly provided by different manufacturers. Those manufacturers typically do not report tolerance and variability of these devices. It is known that the characteristics of those devices are changing over time, like the light bulb.

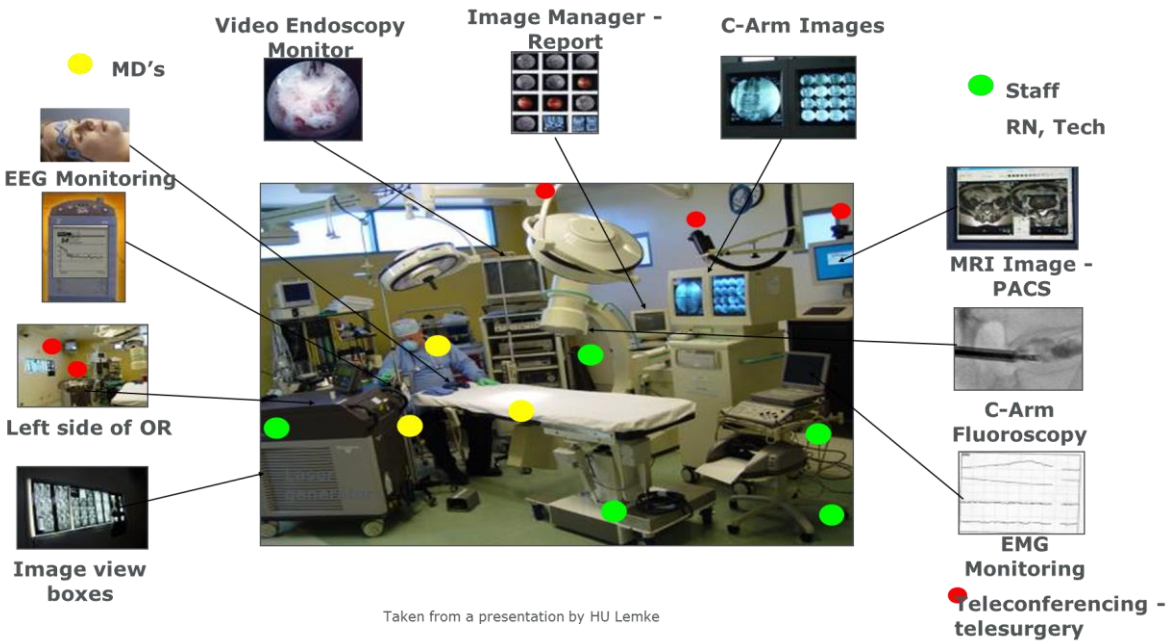

Figure 14: Typical devices in an operating room

To the best of our knowledge, no studies have been done to quantify and qualify the variability and / or the degradation of those devices over time. And it is not known however how large these changes are and what the causes and the main driving factors are. As independent devices are used in such system, the end-to-end variability of the total system will only increase.

Some practitioners are advising to replace a camera after 6 years or after 1500 to 2000 examinations [Systchenko]. This is a rough estimate taking into account various parameters (maintenance cost, security, reliability etc.). These estimates are also limited to the device itself.

6.4.2 Technical State of the Art

In endoscopy as for every medical imaging modality, color rendering plays an important role. Endoscopic images provide color images from inside the body. Following the observed region or organ of interest, colors can be very different: the stomach contains pinkish colors, the small intestine pinkish-yellowish colors [Systchenko Yasushi] etc.

When looking for abnormalities, colors play an important role: for instance white colors will be typical of scars and ulcerations; black for necrotic aspect; red for hemorrhagic; blue for a bruise [Vahedi].

Also, artificial colors can be extremely useful to highlight abnormalities:

- Fluorescence lighting can be used [Tajiri] to highlight tumors, as illustrated below.

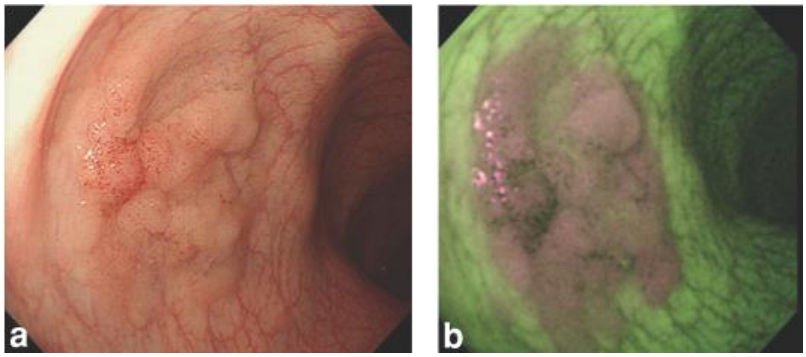

Figure 15: Example of the highlight of a tumor thanks to fluorescent lighting (left: normal lighting; right: fluorescent lighting). Source: [Tajiri]

- Artificial colorations, by means of dyes for instance, can be used to improve the detection of lesions [Dray] [Vahedi]. For instance Indigocarmin is typically used to highlight the surface relief, as illustrated below.

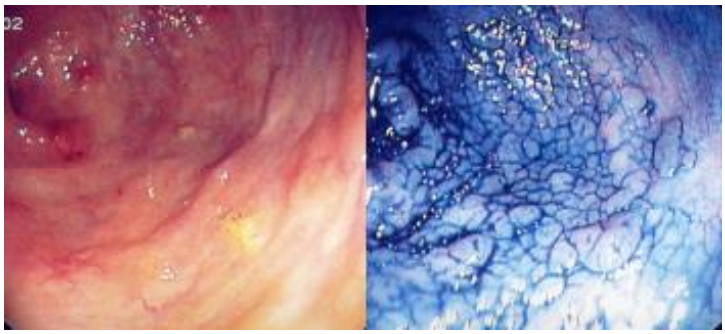

Figure 16: Example of artificial colors with Indigocarmin. Source: [Vahedi]

For clinical practice, it is crucial to ensure true color rendering for the acquired images, ensuring a consistent color rendering over time, whatever are the acquisition and display devices used. This is important to compare examination over time [Delmotte], segmenting efficiently the images and increasing the reliability of the diagnostic.

6.4.3 Usage in intervention and treatment evaluation

<u>The need for a calibration standard for endoscopic images</u>
To the best of our knowledge, there is currently no calibration standard for endoscopic images to ensure true and consistent color rendering of inside the body, although the literature demonstrated the need for it [Haneishi] [Hiroyuki] [Yokoi] [Yamaguchi2013] [Heki] [Billmann] [Constantinou2013] [Yamaguchi2001].

Color rendering will be influenced by the display used in combination with the camera; by the type of lamp; their aging etc. Focusing on the results of the presentation of [Yokoi], the general conclusion from the questioned people is clear regarding the

image rendering in endoscopy: each monitor renders colors differently, and in the case of laparoscopy, this can have an influence on the diagnosis.

Another conclusion of this study demonstrates the clear need to have a standardized color representation and that there is a need to have color management for endoscopy. The study in [Ref Miyake], conducted with 2 skilled physicians, shows the importance of colors for endoscopic images. [Billmann] conducted a study demonstrating that a color deterioration of laparoscopic images result in an increase of the time needed to achieve the task.

[Neofytou2007b] [Constantinou2009] [Neofytou2007] demonstrated that gamma color correction is a necessary pre-processing for CAD to differentiate normal and abnormal endometrial tissue in the early stage of gynecological cancer. The AAPM TG196 [Flynn] points out that a color standardization should be introduced in endoscopy. [Yokoi2006] proposed color standardization for endoscopy examinations.

The work presented in [Haneishi] details a post-process image adjustment to do color correction on endoscopic images, but this process is specific to the review of mucous membrane, and is a 3*3 matrix correction. And as far as we know, only limited research have been made so far to standardize the color rendering of input medical device to ensure true color rendering [Li2006] [Yamaguchi2011] [Grana] [Wee] [Haeghen2000] [Haeghen2006]. And none of them are taking into account the display used to visualize the acquired images. However, it is worth noticing that some work has been done to reduce endoscopic images distortions [Rdf2013a] [Wurzbacher] [Barreto] [Zhang2000] [Wengert] [Wu] [Shahidi], but this does not take into account color fidelity.

White-balancing calibration procedure
Currently, the only calibration-step performed [Cotton] [Saxena] is a white-balancing, performed by pointing the camera to a white-paper. Then the user is manually adjusting the parameters of the display to tune the colors according to its own preferences. He will typically modify the following parameters on the display: luminance, contrast, display function, white point by changing individual red green and blue, gamma. This is done prior to each examination.

Conclusion
Some manufacturers [Oev261h] are advising to use their camera with their display, but here as well, it is only claimed that the display is calibrated to ensure a good color rendering, but no calibration procedure is described to redo it. And if the display is changed, there is a high chance that the colors will not be rendered the same way (different gamut etc.).

Finally, no studies have been done to describe the use-cases, the requirements and the workflow to perform a reliable calibration of those devices, while having the possibility for the surgeon to use its own preferences. Also, those individual preferences have not been studied yet.

6.4.4 BENEFIT updates

Barco is active in the DICOM working group and AAPM Task Group 196 – Requirements and methods for color displays in medicine. Greyscale calibration (DICOM GSDF) is not sufficient to guarantee consistent and qualitative color visualization. A standard that describes how color medical images need to be visualized does not yet exist. Recently a proposal has been made for a "Color Standard Display Function" (CSDF), an extension of DICOM GSDF towards color.

7 Bibliography on Imaging Procedures

- Barreto2009: Barreto, J.P., Roquette, J., Sturm, P. and Fonseca, F. 2009. Automatic Camera Calibration Applied to Medical Endoscopy. (2009).
- Billmann: Billmann F.; 2011. Evaluation of Laparoscopic Performance: a Study on the Effect of Image Color.
- Bruschke AVG, Wijers TS, Kolsters W, Landmann J. The anatomic evolution of coronary artery disease demonstrated by coronary arteriography in 256 nonoperated patients. Circulation 1981; 63(3):527-536.
- Constantinou2009 : Constantinou, I. ; Koumourou C. ; Neofytou M. ; Tanos V. ; Pattichis C. ; Kyriakou E. ; 2009. An Integrated CAD System Facilitating the Endometrial Cancer Diagnosis.
- Constantinou2013: Constantinou I.; Neofytou M.; Tanos V.; Pattichis M.; 2013. A Comparison of Color Correction Algorithms for Endoscopic Cameras.
- Cotton: Cotton P.; Williams C.; 2008. Practical Gastrointestinal Endoscopy.
- Delmotte J-S; 2012. Gestion, reproduction et stockage des images en endoscopie.
- Dray: Dray X; Camus-Duboc M; Marteau P; 2010. Pourquoi et comment colorer la muqueuse en endoscopie?
- Flynn: Flynn M.; Samei E.; Roehrig H.; 2010. Color Monitors for Medical Workstations.
- Grana: Grana C.; Pellacani G.; Seidenari S.; 2005. Practical color calibration for dermoscopy, applied to a digital epilumescence microscope.
- Geijer H. Radiation dose and image quality in diagnostic radiology. Optimalization of the dose-image quality relationship with clinical experience from scoliosis radiography, coronary intervention and a flat panel digital detector. Acta Radiol Suppl 2002; 43:1-43.
- Haeghen2000: Haeghen, Y.V., Naeyaert, J.M., Lemahieu, I. and Philips, W. 2000. An imaging system with calibrated color image acquisition for use in dermatology (2000).
- Haeghen2006: Haeghen, Y.V. and Naeyaert, J.M. 2006. Consistent Cutaneous Imaging With commercial Digital Cameras. (2006).
- Haneishi: Haneishi H; Shiobara T.; Miyake Y.; 1995. Color correction for colorimetric color reproduction in an electronic endoscope.
- Heki: Heki T.; 2013. Color management of endoscopic images.
- Hiroyuki: Hiroyuki, H. 2013. Color Imaging in Endoscopy and Laparoscopy. Olympus.
- Holmes DR Jr, Laskey WK, Wondrow MA, Cusma JT. Flat-panel detectors in the cardiac catheterization laboratory: Revolution or evolution-What are the issues? Cathet Cardiovasc Intervent 2004; 63:324-330.
- Jukema JW, Bruschke AVG, Reiber JHC. Lessons learned from angiographic coronary atherosclerosis trials. In: Reiber JHC, van der Wall EE, editors. Cardiovascular Imaging. Dordrecht/Boston/London: Kluwer Academic Publishers, 1996: 119-132.
- Lansky AJ, Desai KJ, Bonon R, Koning G, Tuinenburg J, , Reiber JHC. Quantitative coronary angiography methodology in vascular brachytherapyII. In: Waksman R, editor. Vascular Brachytherapy, Third Edition. Amronk, NY: Futura Publishing Co., Inc, 2002:543-562.
- Li2006: Li, W., Soto-Thompson, M. and Gustafsson, U. 2006. A new image calibration system in digital colposcopy. Optical Society of America. (2006).
- Miyake: Miyake Y.; Haneishi H.; 1997. Computer Simulation for Improvement of Color Reproduction in Electroni Endoscopes.
- Neofytou2007: Neofytou M.; Tanos V.; Pattichis M. ; Pattichis C. ; Kyriacou E. ; Koutsouris D. ; 2007. A Standardized protocol for texture feature analysis of endoscopic images in gynecological cancer.

- Neofytou2007b: Neofytou M.S.; Tanos V.; Pattichis M.S.; Pattichis C.S.; Kyriacou E.C.; Pavlopoulos S.; 2007. Color Based Texture - Classification of Hysteroscopy Images of the Endometrium.
- Oudkerk (ed.): Coronary Radiology 2nd Edition, Chapter 2.2 QCA / J.H.C. Reiber, et al.: Chapter Coronary Radiology, Springer-Verlag, 2007.
- Oev261h:OEV261H - High definition LCD monitor.
- Rdf2013a: http://arthronav.isr.uc.pt/rdfixer/
- Reiber JHC, Schiemanck L, van der Zwet PM, Goedhart B, Koning G, et al. State of the art in quantitative coronary arteriography as of 1996. In: Reiber JHC, van der Wall EE, editors. Cardiovascular Imaging. Dordrecht: Kluwer Academic Publishers, 1996:39-56.
- Saxena: Saxena, A.K. and Hollwarth, M.E. 2009. Essential of Pediatric Endoscopic Surgery. Springer.
- Shahidi: Shahidi R.; Bax M.; Maurer C.; Johnson J. ; Wilkinson E. ; Wang B. ; West J.; Citardi M.; Manwaring K.; Khadem R.; 2002. Implementation, Calibration and Accuracy Testing of an Image-Enhanced Endoscopy System.
- Systchenko: Systchenko, R. and Maugendre, N. 2012. Renouvellement des endoscopes: quand, comment, pourquoi?
- Tajiri: Tajiri, H; Niwa, H; 2008. Recent Advances in Electronic Endoscopes: Image-Enhanced endoscopy.
- Tsapaki V, Kottou S, Kollaros N, Dafnomilli P, Koutelou M, Vano E, et al. Comparison of a conventional and flat-panel digital system in interventional cardiology procedures. Br J Radiol 2004; 77:562-577.
- Vahedi, K; 2007. Lésions endoscopiques du tractus digestif: description, classification.
- Wee: Wee A.; Lindsey D.; Kuo S.; Johnston W.; 2006. Color Accuracy of Commercial Digital Cameras for User in Dentistry.
- Wengert: Wengert C.; Reeff M.; Cattin P.; Székely G.; 2005. Fully Automatic Endoscope Calibration for Intra-operational Use.
- Wu: Wu C.; Jaramaz B.; Narasimhan S.; 2009. A Full Geometric and Photometric Calibration Method for Oblique-viewing Endoscope.
- Wurzbacher: Wurzbacher T.; Voigt I.; Schwarz R.; Döllinger M.; Hoppe U.; Penne J.; Eysholdt U.; Lohscheller J.; 2008. Calibration of laryngeal endoscopic high-speed image sequences by an automated detection of parallel laser line projections.
- Yasushi: Vu, H.; Yagi, Y.; Echigo, T.; Shiba, M.; Higuchi, K.; Arakawa, T.; Yagi, K.; 2010. Color analysis for Segmenting Digestive Organs in VCE.
- Yamaguchi2001: Yamaguchi M.; 2001. Medical Application of a Color Reproduction System with a Multispectral Camera.
- Yamaguchi2011: Yamaguchi, M., Murakami, Y., Komiya, Y., Kanno, Y., Kishimoto, J., Iwama, R., Hashizume, H., Aihara, M. and Furukawa, M. 2011. Video-Telemedicine with Reliable Color Based on Multispectral Technology. Advances in Telemedicine. (2011).
- Yamaguchi2013: Yamaguchi, M.; 2013. High-fidelity color reproduction and multispectral medical imaging.
- Yokoi2006: Yokoi H.; Fujino M.A.; 2006. Activities for Endoscopy Information Systems Standardization in Japan.
- Yokoi: Yokoi, H. 2013. Overview of Endoscopy and Laparoscopy.
- Zhang2000: Zhang Z.; 2000. A Flexible New Technique for Camera Calibration.
- van der Zwet PMJ, Meyer DJ, Reiber JHC. Automated and accurate assessment of the distribution, magnitude, and direction of pincushion distortion in angiographic images. Invest Radiol 1995; 30:204-213.